



**RADIATION DOSE AND CANCER RISK
ESTIMATES FROM TUBERCULOSIS
INFECTIONS IMAGING**

OLUWABAMISE ADELEYE

2018

**RADIATION DOSE AND CANCER RISK
ESTIMATES FROM TUBERCULOSIS INFECTIONS
IMAGING**

By

OLUWABAMISE ADELEYE

Supervisor: Prof. Naven Chetty

Submitted in partial fulfillment of the requirements for the

degree of Doctor of Philosophy in the

School of Chemistry and Physics

College of Agriculture, Engineering and Science

University of KwaZulu-Natal

Pietermaritzburg Campus

South Africa

2018

ABSTRACT

Radiological examinations in the form of Computed Tomography (CT) and Positron Emission Tomography (PET) integrated with CT (PET/CT) contributions to accurate diagnosis, treatment planning, staging of fever of unknown origin, inflammatory diseases are increasingly reported. Although these devices offer cross-sectional views and 3D reconstructions with a high clinical assessment of many infectious diseases deep within the body compared with other imaging modalities, there are concerns regarding the associated radiation dose to the patient undergoing these imaging techniques. Studies have shown that patient doses from CT procedures are considerably larger than those from other diagnostic X-ray examinations, while a PET/CT examination causes both internal (γ - ray) and external (X-ray) radiation from radiopharmaceutical administration and CT acquisition.

Additionally, the number of CT or PET/CT systems available on the market has increased substantially and new models are being developed and released on a continuous basis. Consequently, scanning techniques have become more sophisticated and complicated, with radiologists facing difficulties in the appropriate adjustment of scanning parameters to patient size and anatomy. Considering the wide variability in body size in the population, lack of optimized protocols could be an additional source of increased dose with a corresponding

increase in cancer risks. In view of the significant benefits from properly conducted medical exposures, and the unavoidable harmful potential effects, it was the interest of this work to quantify the level of radiation exposure to patients, the scanning parameters that significantly affect exposures, the implication of appropriate selection of exposure parameters depending on the diagnostic requirements, and the potential harm, if any, does the typical use of generic protocols have on the health of patients exposed to each one of the modalities. We also explored the radiation protection practices in both types of procedures.

Radiation doses from CT procedures were estimated using Monte Carlo (MC) simulation software, while the Dose coefficients recommended in the International Commission on Radiological Protection (ICRP) publication 106 were used to calculate the doses from a PET scan. The Lifetime Attributable Risk (LAR) of cancer incidence associated with these doses was determined using the formalism implemented in the Biological Effects of Ionizing Radiation (BEIR) VII report of National Research Council, which incorporated the magnitude of radiation exposure, sex, and patient age at the time of exposure.

The investigation of the effect of generic protocols on the magnitude of patient doses and the lifetime risk of cancer during CT examinations from different manufacturer models reveals a significantly different ($P < 0.05$) in organ doses between the CT scanners. A high and statistically significant correlation was observed between estimated lifetime cancer risk for both male ($r^2 = 0.943$, $P < 0.05$) and female patients ($r^2 = 0.989$, $P < 0.05$). The risk variation between the scanners was slightly higher than 2% for all ages but was much smaller for specific ages for male and female patients (0.2% and 0.7% respectively). The related increase in cancer risk though less than 1% emphasized the need for optimized scanner protocols, that

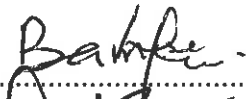
is, exposure protocols that lead to an acceptable image quality for patient-specific indication, based on the individual scanner characteristics as opposed to generic practices.

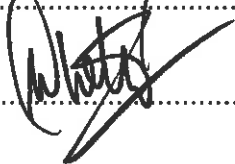
The influence of specific CT model and protocols on the total absorbed radiation dose from a ^{18}F -FDG PET/CT procedure was also investigated in a bid to assess if the changes in CT model and protocols have any significant effect on the overall PET/CT dose, and to analyse possible parameters affecting the CT component radiation dose. Results showed a difference of 4.3%-15% for the Low-dose and 4.1%-11% for the Standard dose scans in the total PET/CT dose between the two systems considered. However, the CT component contributions were not significantly different. The slight variations in the effective dose contribution from the CT component for both PET/CT systems were due to clinical technique differences and type of scanners.

PREFACE

The work described in this thesis was carried out by Oluwabamise Adeleye, under the supervision of Professor Naven Chetty in the School of Chemistry and Physics, University of KwaZulu-Natal, Pietermaritzburg..

The entire work, unless otherwise indicated, is my original work and has not been submitted in part, or in whole, to any other University for degree purpose. Where use has been made of the work of others, it is duly acknowledged in the text.

Signature (Student):.....  Date: 4/09/2018

Signature (Supervisor):.....  Date: 5/09/2018

DECLARATION: PLAGIARISM

I, OLUWABAMISE ADELEYE, declare that:

(i) The research reported in this thesis, except where otherwise indicated; is my original research.

(ii) This thesis has not been submitted in full or in part for any degree or examination to any other university.

(iii) This thesis does not contain other persons' data, pictures, graphs or other information, unless specifically acknowledged as being sourced from other persons.

(iv) This thesis does not contain other persons writing, unless specifically acknowledged as being sourced from other researchers. Where other written sources have been quoted, then:

a) Their words have been re-written but the general information attributed to them has been referenced.

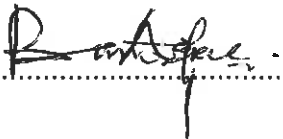
b) Where their exact words have been used, their writing has been placed inside quotation marks, and referenced.

(v) Where I have reproduced a publication of which I am an author, I have indicated which part of the publication was contributed by me and have acknowledged other authors contri-

bution.

(vi) This thesis is primarily a collection of material, prepared by myself, published as journal articles or presented as a poster and oral presentations at conferences. In some cases, additional material has been included.

(vii) This thesis does not contain text, graphics or tables copied and pasted from the internet, unless specifically acknowledged, and the source being detailed in the thesis and in the References sections.

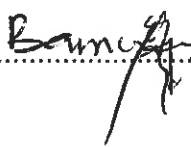
Signed:.....

Date:.....4 / 09 / 2018

DECLARATION 2-PUBLICATIONS

Details of contribution to publications that form part and/or include research presented in this thesis. The first author(student)carried out the experimental work, data collection and manuscript preparation, under the guidance of the second author (supervisor).

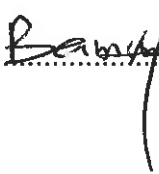
1. B. Adeleye, N. Chetty, Radiation dose and cancer risk estimates in helical CT for pulmonary tuberculosis infections. *Open Physics*,15(2017)769–776.
2. B. Adeleye, N. Chetty, Radiation dose from 18F-FDG PET/CT procedures: Influence of specific CT model and protocols. *Radioprotection*, in press, doi:10.1051/radiopro/2018009
3. B. Adeleye, N. Chetty, Influence of specific CT protocols on cancer risk of exposed patients (In preparation).

Signed:.....  4/09/2018

CONFERENCE CONTRIBUTIONS

1. B. Adeleye, N. Chetty, Radiation dose and cancer risk estimates in helical CT scan with same acquisition protocol: a comparative study. College of Agriculture, Engineering, and Science. Research day. 26 October 2017. University Of KwaZulu-Natal, Westville, South Africa.

2. B. Adeleye, N. Chetty, Radiation dose from 18F-FDG PET/CT procedures: Influence of specific CT model and protocols. Journal of Medical Physics. The 17th Asia-Oceania Congress of Medical Physics (AOCMP 2017) SMS Medical College, Jaipur, India, 4-7 November 2017.

Signed:.....  4/09/2018

Dedication

To my Parents

Mr and Mrs Felix A. Adeleye

I dedicate this work.

Acknowledgements

All glory, honour, and praise to the LORD GOD ALMIGHTY for his mercies and grace upon my life, if it had not been the Lord who was on my side.., none of this would be possible. Hallowed be thy name.

I acknowledge with gratitude my supervisor, Prof. Naven Chetty, for his guidance and kind consideration during the course of this research. I am highly indebted to him for his motivation, moral and financial support that has helped me hitherto. I could not have imagined having a better supervisor for my Ph.D. study. I pray for success in his life career.

My sincere appreciation goes to my parents Mr & Mrs F. A. Adeleye, what a blessing it had been to be born of you, I owe so much to you Dad & Mum. I pray the good lord will continually keep you for me. Thanks for everything. To my inestimable brothers, Abayomi and Ifeoluwa, Guys thanks for your continuous encouragement and prayers.

I acknowledge my friends and colleagues in the School of Chemistry & Physics, UKZN, PMB campus, in particular, the biomedical optics and atmospheric research group for their support and assistance throughout my study. Messrs Karl Penzhorn and Ravin Sivraman are also well appreciated.

Special thanks to Pastor & Mrs D.A Adeleye, the Ajalas, the Faboyas, and Mr & Mrs Bankole Bello for their unalloyed supports and well wishes. May Christ meet you all at your very point of needs.

My unreserved appreciation goes to members of DLCF, Pietermaritzburg. Thanks for your prayers and love. Finally, to all my friends right here in South Africa as well as in Nigeria who have directly or indirectly contributed to the successful completion of this work, your love and care during this period will remain indelible on my mind. Thanks for been there for me.

God bless you All.

List of Abbreviation and symbols

ACD	Annihilation coincidence detection
AEC	Automatic exposure control
AFB	Acid-fast bacilli
AIDS	Acquired Immune Deficiency Syndrome
ALARA	As Low As Reasonably Achievable
BEIR	Biological Effects of Ionizing Radiation
BGO	Bismuth germanate oxide
CD4	Cluster of Differentiation 4
CT	Computed Tomography
CXR	Chest X-ray
$CTDI_{vol}$	volume CT dose index
DAS	Digital Acquisition System
DNA	Deoxyribonucleic Acid
DLP	Dose-Length Product
DRLs	Diagnostic Reference Levels
e^+	Positron charge
e^-	Electron charge
E_0	Incident photon energy
E_S	scattered photon energy

E_B	Binding energy
ED	Effective dose
ELF	Extremely Low-Frequency
^{18}F -FDG	2-deoxy-2-[fluorine-18]fluoro- D-glucose
FOV	Field of View
HBC	High-Burden Countries
HIV	Human Immunodeficiency Virus
IGRA	Interferon Gamma Release Assay
ICRP	International Commission on Radiological Protection
LAM	Lipoarabinomannan
LAR	Lifetime Attributable Risk
LET	Linear Energy Transfer
LYSO	Lutetium-yttrium oxyorthosilicate
MBq	Megabecquerel
MDR	Multi-Drug Resistant
MIRD	Medical Internal Radiation Dose
MTB	Mycobacterium tuberculosis
NIR	Non-Ionizing radiation
PET	Positron Emission Tomography
PTB	Pulmonary tuberculosis
RPW	Radiation Profile Width

SUV_{max}	maximal standardized uptakes values
TB	Tuberculosis
TLD	Thermoluminescent Dosimeters
WHO	World Health Organization

List of figures

Figure	Page
Fig. 1.1 Pie chart showing exposure sources to the United States population	4
Fig. 2.1 The electromagnetic spectrum as a function of wavelength, frequency, and energy.	12
Fig. 2.2 Schematic diagram of the pair production process	17
Fig. 2.3 A general dose-response relationship for deterministic effects	19
Fig. 2.4 Direct and indirect actions of ionizing radiations	22
Fig. 2.5 Schematic representation of a modern CT scanner	24
Fig. 2.6 Radionuclide decay, positron (β^+) emission, multiple scatter in tissue, annihilation with electron, and production of two back-to-back 511 keV annihilation photons	26
Fig. 2.7 Example of tumor localization and hardware image alignment with a PET/CT scanner	33
Fig. 3.1 Estimated lifetime risk of cancer with respect to age from a single standard computerized tomography dose for diagnosis of pulmonary tuberculosis infections in male patients	61

Fig. 3.2 Estimated lifetime risk of cancer with respect to age from a single standard computerized tomography dose for diagnosis of pulmonary tuberculosis infections in female patients	62
Fig. 4.1 The ADAM and EVA phantoms of “CT-expo” used for CT dosimetry calculations.	83
Fig. 4.2 Mean Effective Dose values for Systems I and II .	88

List of Tables

Table	Page
Table 3.1 Summary of the technical parameters used in three 16- slice computed tomography scanners evaluated in this study	56
Table 3.2 Anatomical extent of computed tomographic examinations using CT-Expo mathematical phantoms	57
Table 3.3 Estimated dose (mSv) from a single helical CT scan for diagnosis of pulmonary tuberculosis with three 16-slice scanners	60
Table 3.4 The Contributions of organs exposed to the highest radiation (Breasts and Lungs) for female patients	63
Table 3.5 The Contributions of organs exposed to the highest radiation (Lungs) for male patients	64
Table 4.1 Standard clinically applied CT exposure parameters used on different PET/CT systems	81
Table 4.2 Organs and Tissues equivalent dose D_T from administered ^{18}F -FDG activity and their contribution $W_T * D_T$ to the average PET effective dose	87

Contents

PREFACE	iv
DECLARATION: PLAGIARISM	v
DECLARATION 2-PUBLICATIONS	vii
List of figures	xvi
List of tables	xviii
1 INTRODUCTION	1
1.1 Research Motivation	4
1.2 Aims and Objectives of the thesis	6
1.3 Organization of the thesis	6
2 LITERATURE REVIEW	11

2.1	Radiations and its classification	11
2.1.1	Ionising Radiations	12
2.1.2	Non-Ionizing Radiations	13
2.2	Mechanisms of ionizing radiation interactions with matter	13
2.2.1	Rayleigh scattering	14
2.2.2	Compton scattering	14
2.2.3	Photoelectric effect	15
2.2.4	Pair production	16
2.3	Biological Effects of Ionizing Radiations	17
2.3.1	Deterministic and stochastic effects of ionizing radiations	18
2.3.2	Mechanisms of ionizing radiation damage to the cells	21
2.4	History and basic principles of CT and PET/CT imaging	23
2.4.1	CT Imaging	23
2.4.2	PET/CT Imaging	25
2.5	Radiation dose from ^{18}F -FDG-PET/CT procedures	26
2.6	Role of ^{18}F -FDG-PET/CT imaging in TB diagnosis	29
2.7	The significance of CT in FDG-PET/CT imaging	31
2.8	Factors affecting patient dose in computed tomography	34

2.8.1	Scanner geometry	34
2.8.2	Beam collimation	35
2.8.3	Pitch factor	36
2.8.4	X-ray beam-shaping filters	36
2.8.5	Tube current (mA) and tube current-time product (mAs)	37
2.8.6	Tube Potential (kVp)	38
2.8.7	Scan length	38
2.9	Radiation Protection Principles	39

3 RADIATION DOSE AND CANCER RISK ESTIMATES IN HELICAL CT FOR PULMONARY TUBERCULOSIS INFECTIONS **51**

3.1	Abstract	52
3.2	Introduction	53
3.3	Materials and Methods	54
3.3.1	CT models and protocols	54
3.3.2	Dose assessment	55
3.3.3	Calculation of the attributable risk of cancer	57
3.4	Results	58

3.4.1	Organ-specific and effective doses	58
3.4.2	Attributable risk of cancer	59
3.5	Discussion	65
3.6	Conclusions	69
4	RADIATION DOSE FROM ^{18}F-FDG PET/CT PROCEDURES: INFLUENCE OF SPECIFIC CT MODEL AND PROTOCOLS	76
4.1	Abstract	77
4.2	Introduction	78
4.3	MATERIALS AND METHODS	79
4.3.1	PET/CT System and Protocols	79
4.3.2	CT dosimetry	81
4.3.3	Internal dosimetry	84
4.3.4	Data analysis	84
4.4	Results	85
4.5	Discussion	89
4.6	Conclusions	92
5	Conclusion and future work	99

5.1 Summary 99

5.2 Future work 101

Chapter 1

INTRODUCTION

Tuberculosis (TB) is a chronic granulomatous infection caused by the bacterium *Mycobacterium tuberculosis* [1, 2]. Globally, TB continues to be one of the leading infectious causes of morbidity and mortality, accounting for an estimated 9 million cases and 1.5 million deaths per year [3, 4]. Sub-Saharan Africa countries such as South Africa with a high number of people with immune system problems, such as Acquired Immune Deficiency Syndrome (AIDS) are the most affected. Explicitly, a human immunodeficiency virus (HIV) positive patient has a 20-fold increased risk of contracting TB when compared with HIV negative individual [3, 5]. Despite a global slowing down in new TB cases since 2003 [6], South Africa remains one of the countries with the highest burden of TB, with the World Health Organisation (WHO) statistics giving an estimated incidence of 450,000 cases of active TB in 2013. This is the fourth highest incidence of any country in the world after India, China, and Indonesia. Recent figures from the South African Department of Health are that 73% of the 450,000 incident cases TB patients are HIV positive. The significant improvement in the cure rate (number of cases per 100,000 population where a patient has finished the course of treatment

with bacteriological evidence of success), from 58% in 2005 to 78% in 2014, still fell far short of the global targets of > 85% [7], mainly attributed to late or ineffective diagnostic testing [8]. The delay in diagnosis causes a delay in isolation of the patient with more chance for the infection to spread and thus increasing the severity of the disease [9]. Although TB can affect any organ system in the body, the common and often the initial site of manifestation are the lungs [10, 11].

Despite the enormous burden of TB, current diagnostic methods are woefully inadequate to meet clinical and research needs [12]. The initial diagnostic strategy in adults suspected of having TB is primarily based on history, clinical signs and symptoms, the demonstration of acid-fast bacilli (AFB) on sputum microscopy, and a simple chest radiograph (CXR) mostly for sputum-negative patients not responding to a course of antibiotics [3, 11]. However, the sputum smear microscopy and CXR does not work well to detect TB in HIV positive patients because cavitation and transfer of bacilli into respiratory secretions are markedly reduced due to alteration of the normal host immune response to *Mycobacterium TB*. Additionally, the classical radiographic findings of pulmonary TB, consisting of upper lobe involvement and cavitation without lymphadenopathy are usually only found in HIV positive individuals without severe immunosuppression (CD4 count > 200), with a predominant uncharacteristic radiographic pattern in those with severe immunosuppression (CD4 count < 200) [8].

The insufficiency and low sensitivity of the chest radiographs (CXR) in early detection of TB were reported also by many authors. Lee et al [13] in their study on the role of chest CT scanning in TB outbreak investigation, found the presence of radiographic lesions suggestive of active pulmonary TB in nine patients with normal chest x-ray findings. Uzum et al [14] compared the CXR and thoracic CT findings in children who had contact with adult family members with active pulmonary TB and they found that CXR detected TB in only 7(15%) of 48 children, whereas the thoracic CT scans revealed lymph node enlargement or parenchymal

lesions in 39 (81.2%). Another study by Kim et al [15] found that mediastinal or hilar lymphadenopathy containing low-attenuation nodes with rim enhancement, calcifications, and nodules of bronchogenic spread or miliary nodules a hallmark of tuberculosis in children were missed on chest radiographs. The limitations of these conventional diagnostic approaches have led to heavy reliance on alternative methods of imaging, specifically Computed Tomography (CT) and integrated Positron Emission Tomography (PET)/CT imaging techniques for disease diagnosis, clinical assessment, and treatment follow-up. CT scans provide more accurate information about the extent and distribution of Pulmonary TB through the presence of cavities and subtle lesions than chest radiographs [16, 17]. PET/CT is a non-invasive and sensitive imaging modality that has proven to provide very detailed anatomic-metabolic information on different aspects of tuberculosis consequential of the ability for CT to give anatomic information supporting the metabolic information obtained from PET, thus improving lesion localization and interpretation accuracy [18].

In spite of the tremendous clinical benefits derived from the CT and PET/CT imaging tools, there is growing concern among the patients, public and the scientific community with regards to the associated radiation exposures. Investigation has shown that the amount of radiation exposure applied in a traditional chest CT examination is about 3 to 20 times more than the radiation dosage used for a conventional chest X-ray examination [16], while exposures from PET/CT examinations are relatively higher compared to other imaging modalities based on ionizing radiation, due to the additional external exposure (X-ray) from CT acquisition, in addition to internal exposure (γ - ray) from administered radiopharmaceuticals. As a consequence, CT and PET/CT represent the major contributor of the annual collective dose from medical exposures Figure(1.1)— the largest contribution to population dose from man [19, 20]. With the rapidly expanding quantity of these examinations, a resultant increase in cancer cases can be expected [21-23], thus the deliberate choice to investigate

these high-dose imaging tests.

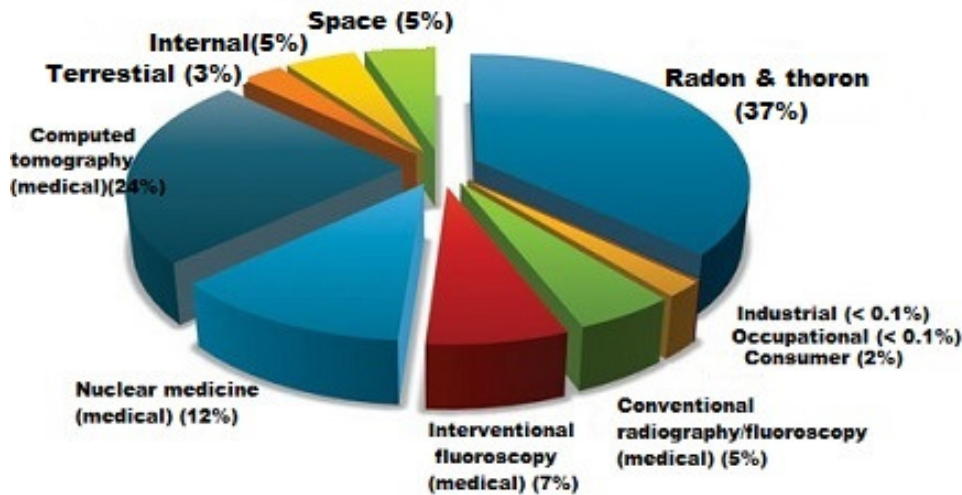


Figure 1.1: Pie chart showing exposure sources of the United States population (NCRP Report 160, 2009) [23]

1.1 Research Motivation

The number of CT or PET/CT devices available on the market has increased substantially and new models are being developed and released on a continuous basis [25,26]. Although these devices offer cross-sectional views and 3-dimensional reconstructions with high diagnostic capability of many infectious and inflammatory disease deep within the body compared with other imaging modalities, scanning techniques have become more sophisticated and complicated, and radiologists are faced with an expanding array of options, including the

selection of exposure parameters such as the tube current, kilovoltage, collimation, and table speed (hence, pitch). Considering the wide variability in body size in the population, careful selections of these parameters are necessary and important to optimize pertinent diagnostic information. It is germane to mention that to the best of our knowledge, despite the increasing demand for these imaging modalities owing to the prevalence of HIV infection and related opportunistic diseases such as tuberculosis infection, there has been no published information regarding any adherence to technical recommendations or guidelines as to when or how they should be utilized and such lack of information reinforces fears about radiation exposure.

In view of the significant benefits from properly conducted medical exposures, and the unavoidable harmful potential effects, periodic radiation dose, and risks assessment are paramount for the optimization of radio-diagnostic procedures and assurance of the application of radiological protection principles. The level of radiation exposure to patients, the scanning parameters that significantly affect exposures, the implication of appropriate selection of exposure parameters depending on the diagnostic requirements, and what potential harm, if any, does the typical use of generic protocols have on the health of patients exposed with each one of the modalities need to be explored and this study has been designed to address this issue. The non-implementation of established imaging protocols suggests a variation of above 2% in lifetime cancer risks.

Furthermore, investigation of the influence of CT scanner and study protocol on the overall PET-CT dose is also analysed. It was proposed that a difference in CT component and study protocol causes no significant effect on the overall dose. The major contribution based on the considered imaging procedure is created by the CT acquisition parameters used. The data presented in this study will constitute a part of the global effort in radiation protection of patients in diagnostic radiology.

1.2 Aims and Objectives of the thesis

The specific objectives of this study are to:

- assess the radiation absorbed dose and effective dose from the CT and integrated PET/CT imaging modalities as a means for the optimization of the radiation protection of patients,
- quantify the potential risk from exposures taking into account organ risk factors and evaluate the influence of age, sex and scan protocol on cancer risk,
- investigate what potential harm, if any, the typical use of generic protocols has on the radiation dose and the corresponding risk for exposed patients,
- analyze the critical adjustable scanning parameters that are determinants of the radiation dose a patient receives for each examination and
- provide recommendations as to the application of each imaging technique for various clinical conditions, to ensure essential diagnostic information is obtained with As Low As Reasonably Achievable (ALARA principle) radiation exposure.

1.3 Organization of the thesis

The structural organization of this thesis is presented in five (5) chapters. Chapter 1 gives the general introduction to this work, the motivation for the study and the specific aims and objectives of the study. A theoretical background (literature review) on the history and basic principles of CT and PET/CT imaging are discussed in chapter 2. The likely biological effects following exposures and overview of factors affecting patient dose from these procedures were also discussed. The contribution of various researchers to patient dose estimation vis-à-vis the commonly used methods such as Thermo-luminescent dosimeters, mathematical modeling

globally and within South Africa is presented. The chapter concludes with a brief review of radiation protection principles. Chapter 3 is a published journal article that focuses on the estimation of the absorbed radiation dose and long-term effects (cancer risks) for exposed patients from helical CT for pulmonary tuberculosis infections. We hypothesize the same scan protocol while focusing on the adjustable scan parameters that are determinants of radiation dose for three 16-slice units. Furthermore, we determine what, if any, correlation exists between dose and cancer risks for each scanner. Chapter 4 quantifies the effects of CT model and exposure protocols on the overall radiation effective dose to patients for commonly performed CT techniques in a ^{18}F -FDG PET/CT examination. The study focused on two PET/CT systems and five CT exposure protocols routinely applied for clinical patients in PET/CT imaging. Additionally, a comprehensive analysis of the influence of selected exposure parameters on radiation dose is also given. The findings of this chapter have been presented at an international conference and are accepted for publication in a learned journal. Lastly, Chapter 5 summarizes the major findings of the study based on each chapter and provides some suggestions for future work.

Bibliography

- [1] Annual Performance Plan 2012/13 – 2014/15”, Department of Health, South Africa 2012 App 2012-2014. Pdf [accessed 22 May 2017].
- [2] Harkirat S., Anana SS., Indrajit LK., Dash AK (2008) Pictorial essay: PET/CT in tuberculosis. *Indian J Radiol Imaging* 18(2): 141–147.
- [3] Sathekge M., Maes A., Van de Wiele C (2013) FDG-PET Imaging in HIV Infection and Tuberculosis. *Semin Nucl Med.* 43(5):349-66.
- [4] Skoura E., Zumla A., Bomanji J., (2015) Imaging in tuberculosis, *Int. J. Infect Dis.* 32: 87–93.
- [5] UNAIDS. Report on the Global AIDS Epidemic. Geneva: UNAIDS; 2008.
- [6] Cullinan K., South Africa has worst TB prevalence in the world – report. Health Systems Trust 2017 report. <http://www.hst.org.za/news/south-africa-has-worsttb-prevalence-world-report> [accessed 22 May 2017].
- [7] Kanabus A., Information about Tuberculosis”, Global Health Education, 2017, <http://www.tbfacts.org/tb-statistics-south-africa/> [accessed 12 June 2017].
- [8] Mendelson M., (2007) Diagnosing tuberculosis in HIV-infected patients: challenges and future prospects. *British Medical Bulletin* 81-82:149-65.

- [9] Shaarawy H., Zeidan M., Nasr A., Nouh M. (2013) Assessment of the role of high resolution computed tomography in the diagnosis of suspected sputum smear negative active pulmonary TB. *Egyptian Journal of Chest Diseases and Tuberculosis* 62: 263–268.
- [10] Harkirat S., Anana SS., Indrajit LK., Dash AK (2008) Pictorial essay: PET/CT in tuberculosis. *Indian J Radiol Imaging* 18(2):141–147.
- [11] Bhalla AS., Goyal A., Guleria R., Gupta AK (2015) Chest tuberculosis: Radiological review and imaging recommendations. *Indian J Radiol Imaging* 25(3):213–225.
- [12] Hanrahan CF, Shah M (2014) Economic challenges associated with tuberculosis diagnostic development. *Expert Rev Pharmacoecon Outcomes Res* 14(4):499–510.
- [13] Lee SW, Jang YS, Park CM, Kang HY, Koh WJ, Yim JJ, Jeon K (2010) The Role of Chest CT Scanning in TB Outbreak Investigation. *Chest* 137(5):1057-64.
- [14] Uzum K, Karahan OI., Dogan S., Coşkun A., Topcu F. (2003) Chest radiography and thoracic computed tomography findings in children who have family members with active pulmonary tuberculosis. *Eur J Radiol.* 48 (3):258-62.
- [15] Kim WS, Moon WK., Kim IO, Lee HJ., Im JG, Yeon KM, Han MC (1997) Pulmonary tuberculosis in children: evaluation with CT. *AJR Am J Roentgenol.* 168(4):1005-9.
- [16] Peng SS, Chan PC, Chang YC, Shih TT (2011) Computed tomography of children with pulmonary Mycobacterium tuberculosis infection. *J Formos Med Assoc.* 110(12):744-9
- [17] Curvo-Semedo L, Teixeira L, Caseiro-Alves F (2005) Tuberculosis of the chest. *Eur. J. Radiol.* 55:158–172

- [18] Ankrah AO, van der Werf TS, de Vries EF., Dierckx RA., Sathekge MM, Glaudemans AW. (2016) PET/CT imaging of Mycobacterium tuberculosis infection. *Clin Transl Imaging* 4:131-144
- [19] Kralik I, Štefanić M, Brkić H, Šarić G, Težak S, Grbac Ivanković S, Griotto N, et.al. (2017) Estimated collective effective dose to the population from nuclear medicine diagnostic procedures in Croatia: A comparison of 2010 and 2015. *PLoS One* 12(6):e0180057.
- [20] Ogbole G.I., (2010) Radiation dose in pediatric computed tomography: risks and benefits. *Ann Ib Postgrad Med.* 8(2): 118–126.
- [21] Brenner D.J., Hall E.J. (2007) Computed tomography — an increasing source of radiation exposure. *N Engl. J. Med.* 357:2277-2284.
- [22] Nievelstein RA, Quarles van Ufford HM, Kwee TC, Bierings MB, Ludwig I, Beek FJ, et.al, (2012) Radiation exposure and mortality risk from CT and PET imaging of patients with malignant lymphoma. *Eur Radiol.* 22:1946–1954
- [23] . Executive Summary Board on Radiation Effects Research — Division on Earth and Life Studies(2006) Health risks from exposure to low levels of ionizing radiation: BEIR VII — Phase 2. National Academy Press, Washington DC
- [24] National Council on Radiation Protection and Measurements (2009). Ionizing radiation exposure of the population of the United States. National Council on Radiation Protection (NCRP) report no. 160. Bethesda, Maryland.
- [25] Workman R.B., (2006) “PET/CT: Essentials for Clinical Practice”, Springer Science & Business Media, LLC, 233 Spring Street, New York, USA.
- [26] Pan J.A., Salerno M. (2016) Clinical Utility and Future Applications of PET/CT and PET/CMR in Cardiology. *Diagnostics (Basel)*,6(3):32.

Chapter 2

LITERATURE REVIEW

In this chapter, we discuss the history and basic principles of the CT and PET/CT imaging techniques and review their roles in the treatment and accurate diagnosis of tuberculosis infections. The different mechanisms of radiation interactions with matter and their respective effects on biological tissues are also presented.

2.1 Radiations and its classification

Radiation is a term used to collectively describe the emission and propagation of energy in the form of waves or particles through space or a material medium [1]. The energies produced either from unstable atoms undergoing radioactive decay or by machines are classified broadly into ionizing or non-ionizing, depending on whether it is sufficient enough to knock electrons off their orbits around atoms, as well as being able to do lower-energy damage such as breaking chemical bonds in molecules [2, 3].

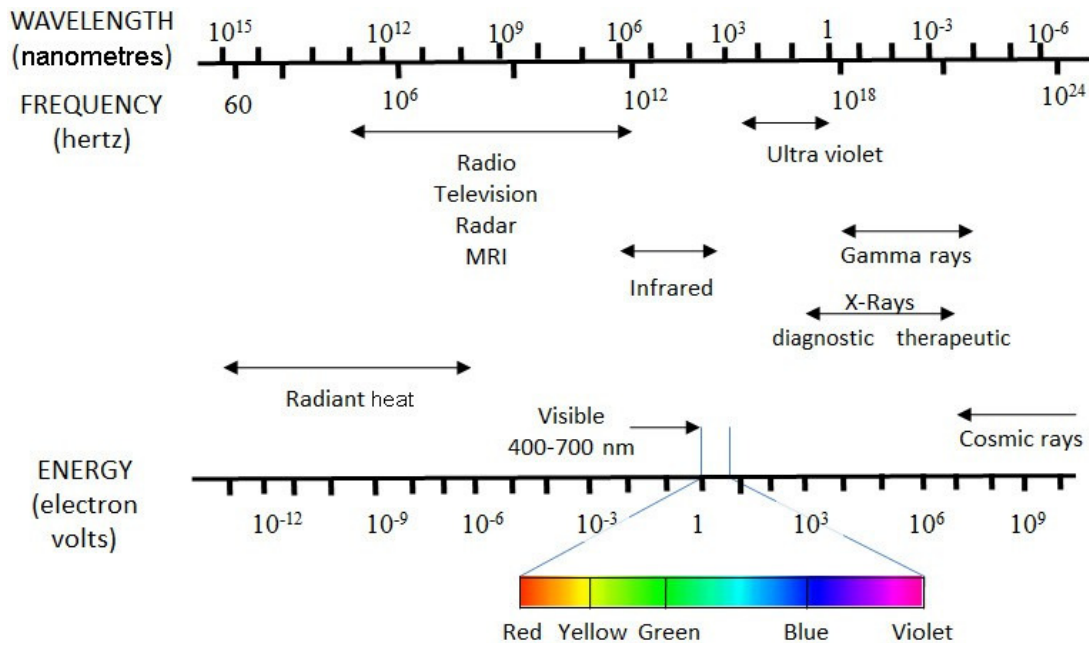


Figure 2.1: The electromagnetic spectrum as a function of wavelength, frequency, and energy.

X-rays and γ - rays comprise the high-energy portion of the spectrum[4]

2.1.1 Ionising Radiations

Ionizing radiation such as gamma(γ) and X-ray are capable of ionizing matter either directly through many small Coulomb (electrostatic) interactions with orbital electrons along its tracks or indirectly from interaction via reactive species released in one or a few interactions in the matter through which they pass [4, 5]. The minimum energy required to ionize an atom, i.e. to remove an electron, is known as the ionization potential. The magnitude ranges from a few electron volts for alkali metals to 12.6 eV for water and 24.5 eV for helium [4].

2.1.2 Non-Ionizing Radiations

Non-Ionizing radiation (NIR) refers to radiative energy capable of producing excitation, but not sufficient energy in comparison to ionizing radiation for charged ions, when passing through matter. They encompass long wavelength (> 100 nm), low photon energy (< 12.4 eV) portion of the electromagnetic spectrum, from 1Hz to 3×10^{15} Hz. The NIR spectrum is divided into two main regions, optical radiation (ultraviolet, visible, and infra-red) and electromagnetic fields separated into radiofrequency (microwave, very high frequency and low-frequency radio wave) [6]. However, NIR are termed as extremely low-frequency (ELF) waves and are not considered to pose a health risk [2].

2.2 Mechanisms of ionizing radiation interactions with matter

Ionizing radiations can actively interact with matter, with the result that energy is transferred to the material [7]. The interactions between the gamma-ray and x-ray photons and matter decreases the intensity (number of photons) of the primary beam traversing through the material- a process called attenuation. The attenuation of a photon beam by an absorbing material is by four basic types of interactions namely: Rayleigh scattering, Compton scattering, Photoelectric effect and Pair production.

2.2.1 Rayleigh scattering

The Rayleigh scattering also known as classical or coherent scattering occurs mainly when very low energy x-ray photons interacts with and excites the total atom causing electrons to vibrate in phase [8]. The oscillating electron re-radiates the energy at the same frequency as the incident photon but with a slightly different direction. In this interaction, no absorption of energy occurs (ionization does not occur). Consequently the only effect is the scattering of the photons at small angles [1, 8]. The probability of this type of scattering occurring is low, about 5% due to the low effective atomic number of soft tissues and is represented by Eqn 2.1.

$$\text{Probability of scatter} \propto \frac{Z^2}{E^2}, \quad (2.1)$$

where Z is the atomic number of the material and E the energy of the incident photon.

2.2.2 Compton scattering

In the Compton process, the photon interacts with an atomic electron as though it were a free electron consequential of the fact that the energy of the bombarding photon (E_0) is much greater than the binding energy of the electron (E) [1]. The partial energy transfer to the electron causes a recoil and emission of a valence electron from the outer orbital shell at an angle θ . Simultaneously, a photon with reduced energy (E_s) is scattered with a trajectory of angle ϕ relative to the trajectory of the incident photon.

By applying the laws of conservation of energy and momentum, the energy of the scattered photon relative to the incident photon for a photon scattering angle ϕ is expressed by equation 2.2 [1]:

$$\frac{E_s}{E_0} = \frac{1}{1 + \alpha(1 - \cos\phi)} \quad (2.2)$$

where, α is the dimensionless ratio E_0/m_0c^2 and m_0c^2 the rest energy of the electron (0.511 MeV). The equation shows that the scattered x-ray energy becomes smaller as the scattering angle increases and at higher incident energies, the effect is amplified.

The scattered photon angle is related to the scattered electron angle by [1, 4]

$$\cot \theta = (1 + \alpha) \tan \frac{\phi}{2} \quad (2.3)$$

2.2.3 Photoelectric effect

In this interaction, the entire energy $h\nu$ of the incident photon is transferred to the absorbing atom resulting in the ejection of an orbital electron in the K, L, M, or N shells. The kinetic energy E of the ejected electron (termed the photoelectron) equals the difference of the incident photon energy $h\nu$, and the electron shell binding energy E_B , [1] i.e.

$$E = h\nu - E_B \quad (2.4)$$

The vacated electron shell though subsequently filled by an electron from a higher energy level with the emission of a characteristic x-ray equal in energy to the difference in electron binding energies of the source electron shell and the final electron shell, creates another vacancy in the process which is also filled from another higher binding energy shell, leading to

an electron cascade where electrons transition between different energy shells [8, 9]. There is also the possibility of emission of Auger electrons (monoenergetic electrons produced by the absorption of the characteristics x-rays) internally by the atom [8]. The probability of photoelectric absorption depends on the photon energy. If the incident photon energy is less than the binding energy of the electron, the photoelectric interaction cannot occur, but if the x-ray energy just equals the electronic binding energy, resonance occurs and the probability of photoelectric effect becomes energetically feasible.

Beyond this point, if the photon energy is increased, the likelihood of photoelectric attenuation decreases approximately as $1/E^3$ [1, 8]. Image contrast is improved with photoelectric interaction since the process amplifies differences in attenuation between tissues with different atomic numbers [9].

2.2.4 Pair production

Pair production can occur when the incident X-ray or γ -ray photon has energy greater than 1.02 MeV, which represents the threshold energy required to create the pair of electrons since the rest mass energy of the electron is equivalent to 0.51 MeV. In this process, the photon interacts strongly with the electromagnetic field of an atomic nucleus and gives up all its energy in the process of creating a pair consisting of both a negative (e^-) and a positive electron (e^+) [1]. The photon energy in excess of 1.02 MeV is shared equally between the e^+/e^- pair as kinetic energy, obeying the law of conservation of energy represented by equation 2.4:

$$h\nu = 2(m_0c^2) + K_{e^+} + K_{e^-}, \quad (2.5)$$

where $h\nu$ is the initial energy of the incident photon, $2(m_0c^2)$ the total rest mass energy of the electron and positron, and K_{e^+} and K_{e^-} their kinetic energies.

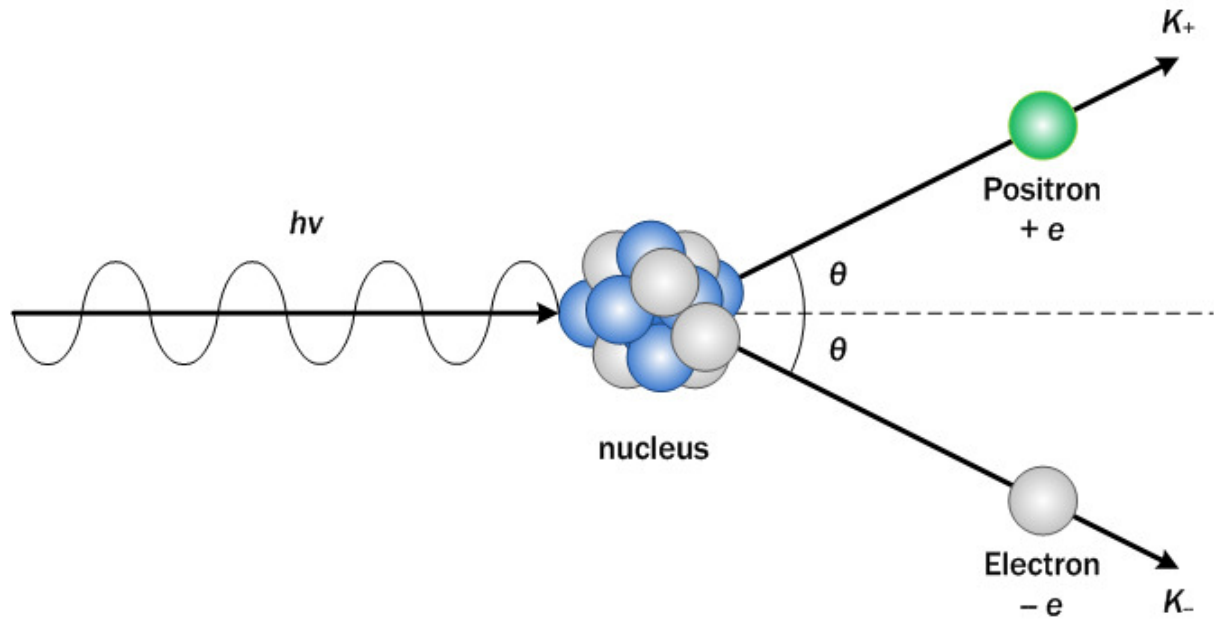


Figure 2.2: Schematic diagram of the pair production process

Once the created positron expends its kinetic energy as it traverses matter, it will combine with any available electron and produce two photons called annihilation radiation, resulting from the conversion of the rest mass energies of the e^+/e^- pair [1, 8]. Pair production occurs at energies well above those used for diagnostic x-ray imaging.

2.3 Biological Effects of Ionizing Radiations

Ionizing radiations with sufficient energy to remove electrons from their atomic or molecular orbital shells in tissues [5], could result in tissue damage and disruption of cellular function at molecular level if received in sufficient quantities over a period. Their effect on the deoxyribonucleic acids (DNA) which control the structure and function of the cell and in turns passes on copies of itself is of major concern [10]. The biological effectiveness depends on the spatial distribution of the energy imparted and the density of ionization per unit path

length of the ionizing particles [11]. The potential biological effects caused by radiation are classified based on their nature and occurring time after exposure [12] as follows:

Acute (short-term) effects: This occurs when the body is exposed to a large dose of radiation (about 10 rad or greater). The exposures could be all at once or from multiple exposures intermittently during a very short time [2]. Instances of acute effects manifest themselves within hours or days, as the body cannot repair or replace cells fast enough from excessive cell damage and grows progressively shorter with an increase in maximum dose received. Examples include reduced blood count, hair loss, nausea, and fatigue [13].

Chronic (long-term) effects: These effects result from the relatively small amount of radiation energy absorbed over a long period of months, years, or lifetime. The exposure could be continuous, e.g. exposure received daily from natural background radiation or off and on routinely over a long time such as occupational radiation exposure [2]. Chronic doses do not result in detectable health effects seen with acute doses consequential of the fact that the body possesses enough time to replace dead or non-functioning cells with healthy ones. Among the long-term effects, thus far observed have been somatic damage, which may result in an increased incidence of cancer, embryological defects, cataracts, and harmful genetic changes for generations after the original radiation damage [2,13].

2.3.1 Deterministic and stochastic effects of ionizing radiations

Radiation effects are also categorized as either deterministic or stochastic:

Deterministic Effects

Also described as tissue reactions are one in which the severity of the effects increases with absorbed dose in affected individuals. These types of effects are characterized by a threshold dose level below which the effect does not occur. The level of the threshold dose is typical of the particular health effect and to a limited extent, the exposed individual. Deterministic risks are rarely seen with diagnostic x-ray or γ - ray based examinations because radiation doses typically do not reach the threshold level [14]. Examples of threshold doses for deterministic effects in some radiosensitivities tissues include 3.5 - 6.0 Gy (sterility) in testis, 2.5-6.0 Gy (infertility) in the ovaries and 5 Gy (cataract formation) in the lens of the eyes [15].

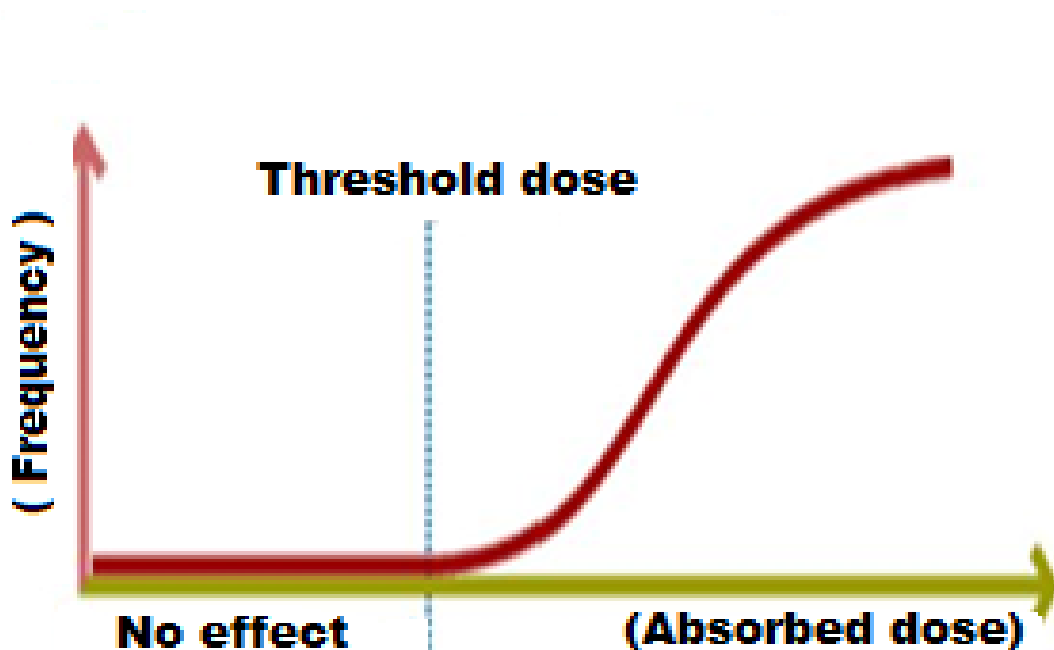


Figure 2.3: A general dose-response relationship for deterministic effects [16]

Stochastic Effects

This type of detrimental effect has a probability that is proportionate to the absorbed dose, but the timing of the effects or their severity in affected individuals does not depend on the magnitude of the dose [1]. They include the detriment-adjusted nominal risk of cancer and heritable effects owing to mutation of reproductive cells. The occurrence of stochastic effects is a consideration with low-dose exposures typically encountered in diagnostic radiology since there is no associated threshold point below which it is relatively certain that an adverse effect cannot occur [14].

Additionally, as stochastic effects can occur in individuals not exposed to radiation above background levels, it can never be determined for certain that an appearance of cancer or genetic effect is due to a specific exposure. The increase in occurrence is provable only by the epidemiological method. The International Commission on Radiological Protection [17], indicates a value of 5.5 % per sievert for cancer and 0.2 % per sievert for heritable effects after exposure to radiation at low dose rate.

2.3.2 Mechanisms of ionizing radiation damage to the cells

The radiation damage to the cells is ascribed to two basic mechanisms direct and indirect actions [7, 18].

Direct Actions

The direct effect proposes that radiation has the potential to interact directly with the target structures (DNA molecule) to cause ionization, thus initiating the chain of events leading to biological damage or even cell death. Surviving damaged cells may later induce carcinogenesis or other abnormalities. Direct actions are dominant for radiations with high linear energy transfer LET (energy loss per unit path length for a charged particle) such as neutrons, protons, or alpha particles owing to the fact that they travel in a straight path as they penetrate tissue due to their relatively large masses in comparison to electrons [12, 18].

Indirect Actions

In indirect action, radiation interacts with atoms or organic molecules in a cell (usually water molecules) being the major constituent in living organisms leading to a rapid production of oxidizing and reducing reactive free radicals such as hydroxyl (HO^*) and also hydroperoxyl (HO_2^*) in oxygenated solutions [18]. These free radicals interact with atoms and molecules within the cells, particularly DNA, to produce chemical modifications and consequently harmful effects [12].

It is estimated that about two-thirds of the radiation-induced damage caused by low linear energy transfer (LET) radiations (sparsely ionizing) such X-ray or γ - ray occurs through indirect action mechanism because water constitutes nearly 70% of the composition of the

cell [18, 19]. The number of free radicals produced depends on the total dose of radiation received. The result of the indirect action of radiation on DNA molecules is the impairment of function or death of the cell. Koturbash et al [20] concluded that when the DNA is attacked, either via direct or indirect action, the ultimate result is the development of biological and physiological alterations which might involve genetic and epigenetic changes in its evolution manifesting themselves seconds or decades later.

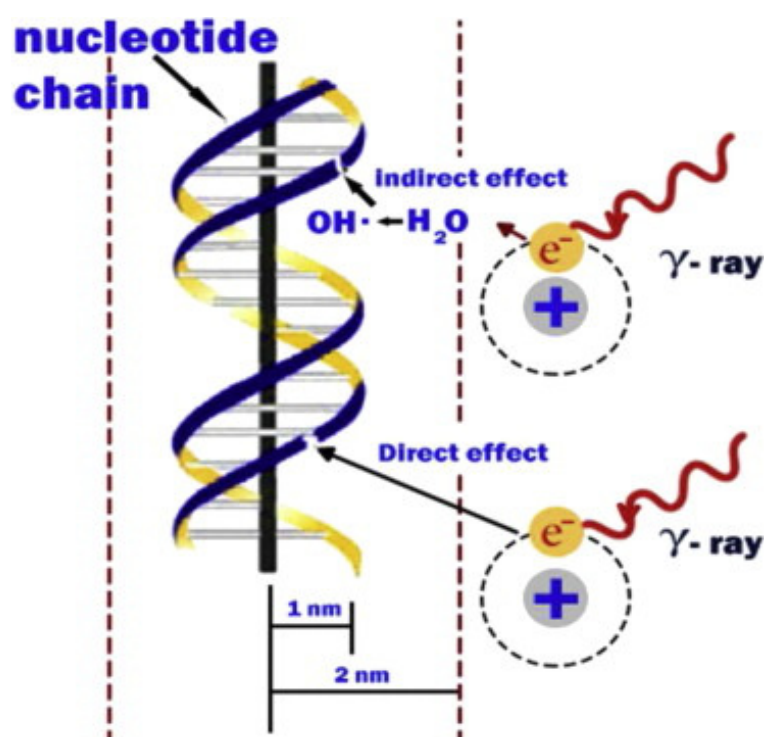


Figure 2.4: Direct and indirect actions of ionizing radiations[20]

2.4 History and basic principles of CT and PET/CT imaging

2.4.1 CT Imaging

CT is an imaging technology consisting of a patient table surrounded by a gantry, which holds the x-ray tube generator, detector array, slip rings, collimators and digital acquisition system (DAS). A 3-dimensional representation of the interior of a patient is generated with multiple x-ray projections as the gantry rotates around the patient [22]. The first CT scanner was invented by Godfrey Hounsfield in the 1970s. Since then, CT technology has developed significantly over the last 20 years, with the advent of spiral CT in the 1990s and the subsequent introduction first of dual-slice CT scanners and then of multi-slice scanners with the capability of generating 16, 64 and 128 slices per rotation [23]. As the x-ray tube rotates around the patient, the x-ray photons generated within the tube are attenuated in the patient's tissue and are captured by the detectors converting it into digital information via the DAS [23]. The attenuation of the x-ray radiation in the patient's tissue followed Lambert's law of absorption [24]:

$$I = I_0 e^{-\mu x}. \quad (2.6)$$

Hence,

$$I = I_0 e^{-\int \mu(x, y) dx}, \quad (2.7)$$

where I is the intensity of the transmitted x-ray beam, I_0 is the intensity of the incident beam, and $\mu(x, y)$ is the linear attenuation coefficient at position (x, y) along the ray path.

The acquired X-ray data is then reconstructed through sophisticated mathematical algorithms to produce a cross-sectional image of the internal structures of the body region scanned for diagnostic use.

The CT image is the measurement and ‘demonstration’ of the linear attenuation coefficients $\mu(x, y)$ of the structures that the x-ray beam interacts with during the examination. The filters are responsible for removing low-energy x-ray photons, thereby reducing patient dose, while the collimators are used to define the slice thickness and localize the x-ray field to the area of interest.

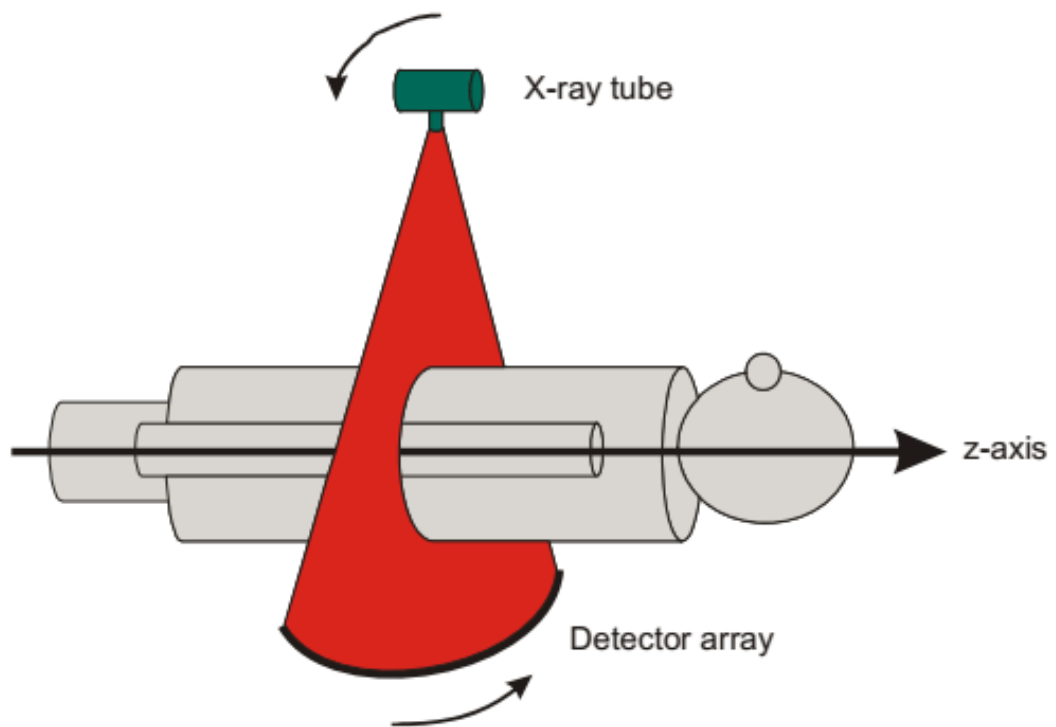


Figure 2.5: Schematic representation of a modern CT scanner; the X-ray tube and detector system rotate together around the patient.[24]

2.4.2 PET/CT Imaging

The demand for more accurate anatomic localization of regions identified on the tracer uptake patterns in PET overextended imaging ranges at reasonable patient exposure levels underlies the main concept of combined PET/CT imaging [26]. PET/CT systems are combinations of three main components: a PET scanner, a CT scanner, and a shared patient bed in a single gantry with the PET components on the reverse side of the rotating support of the CT scanner [27, 28]. The first PET/CT scanner was constructed in 1998 through a collaboration of the National Cancer Institute, CTI PET Systems (Knoxville, Tennessee), and the University of Pittsburgh from independent, previously developed CT and PET scanners [27]. Results from this prototype helped to stimulate further development and construction of combined PET/CT scanners [28]. A typical PET/CT examination starts with the CT scout scan or topogram to define the scan area, followed by a helical CT scan over the range defined on the scout scan, and finally the PET scan [26, 29].

PET image acquisition is based on the annihilation coincidence detection (ACD) of two collinear 511keV photons produced from a radionuclide tagged tracer molecule. Upon administration of very small amounts (pico- or nanomoles) of a radiotracer to the patient it distributes among and within the organs. The radioactive atom of the radiotracer emits positrons which annihilate with a nearby electron after traveling a short distance ($\approx 1mm$) in the tissue. The product of this annihilation is a pair of photons, which following the laws of conservation of energy and momentum are emitted in nearly opposite directions. The energy balance of the two photons can be written as:

$$2(m_0c^2) + K_{e^+} + K_{e^-} = 2h\nu, \quad (2.8)$$

where $2(m_0c^2)$ is the total rest mass energy of the particles, K_{e^+} and K_{e^-} their kinetic energies before collision and $2h\nu$ is the energy after collision.

During the scan millions of coincidence detections are collected by the many photon detectors of the PET scanner surrounding the patient, providing information about the distribution of the radiotracer in tissue.

The CT component provides morphological information and could also be used to correct for the effect of photon attenuation in patient which causes loss of coincidences since the number of measured coincidences depends on the patient's 'radiological' thickness [23].

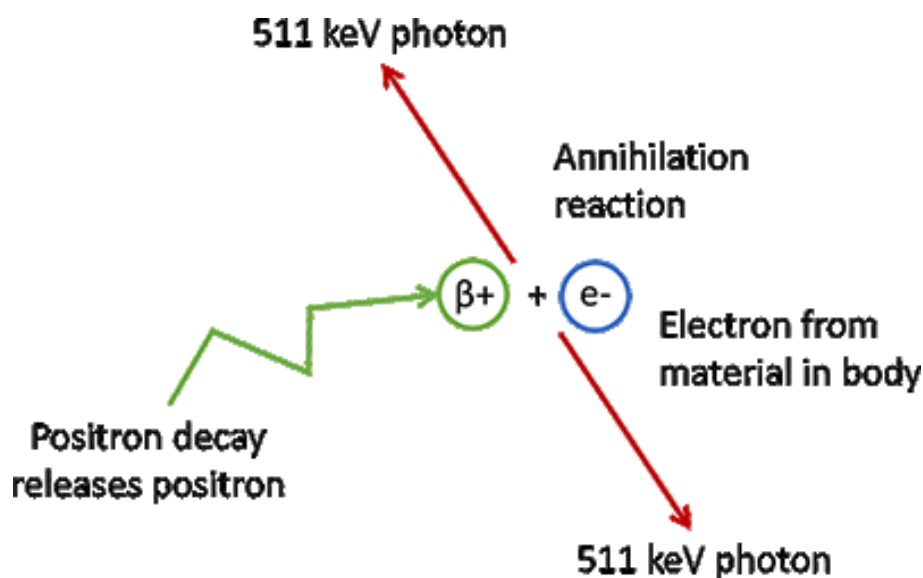


Figure 2.6: Radionuclide decay, positron (β^+) emission, multiple scatter in tissue, annihilation with electron, and production of two back-to-back 511 keV annihilation photons.[29]

2.5 Radiation dose from ^{18}F -FDG-PET/CT procedures

It has long been widely reported that PET/CT examinations especially those involving diagnostic CT, are accompanied by a substantial radiation dose that may enhance the risk of cancer. The evidence for this conclusion is not based on direct proof, but the inference from studies that have estimated the radiation exposure from the procedure. The absorbed dose in FDG PET/CT arises internally (γ - ray) from injected radiopharmaceutical and

externally (X-ray) from CT sources and is predominantly dependent on the strategies for CT usage. For example, Mattson and Soderberg [31] stated that a low-dose CT performed for attenuation correction and anatomical orientation may only account for 50% (2–3 mSv) of the whole PET/CT dose, for an investigation with PET effective dose of 7 mSv (total dose 9–10 mSv). However, in a study to estimate the radiation dose and cancer risk during a whole-body PET/CT scan, Huang et al [32] compared three different CT acquisition protocols using a humanoid (Alderson-Rando) phantom equipped with thermoluminescent dosimeters (TLD-100). They found the total PET/CT effective dose with a diagnostic CT protocol and an administered ^{18}F -FDG activity of 370 MBq to be approximately 32 mSv (81% of the combined dose was attributable to the CT doses).

Brix et al [33] performed a similar study in four German university hospitals. The authors reported effective doses of the order of 23.7 – 26.4 mSv. Their examinations mostly include a diagnostic CT scan, and only in some of the hospitals, a low-dose CT. The diagnostic CT was estimated to deliver 14.1 – 18.6 mSv, while the low-dose CT was reported to contribute 1.3 – 4.5 mSv. They concluded that considering the increased patient exposure compared with individual CT or PET examinations, a judicious medical justification of every PET/CT referral is required. Quinn et al [34] used patient-specific data to characterize the radiation dosimetry of two types of routine whole body PET/CT protocols at their institution. They specifically evaluated the combined PET and CT scan dose for 183 consecutive adult patients who undergo either the standard registration or full dose diagnostic CT techniques. The researchers found that for all standard PET/CT patients, the mean total effective dose was 14 ± 1.3 mSv and mean CT effective dose was 5.0 ± 1.0 mSv, while for all diagnostic PET/CT patients, the mean total effective dose was 24.4 ± 4.3 mSv with mean CT effective dose 15.4 ± 5.0 mSv.

The authors suggested that differences in scanner hardware and software factors at a given

imaging clinic can cause the radiation dose from a standard PET/CT with separate diagnostic CT to be more or less than the radiation dose from a diagnostic PET/CT. They, therefore recommend that incorporating clinic and patient-specific data in dose estimation is important especially for oncology patients who potentially can have many scans and must track cumulative exposure. Many other investigators have evaluated the exposure from ^{18}F -FDG PET/CT procedures. Avramova-Cholakova et al [35] retrospectively collected data on 108 patients from two different PET-CT systems. They reported average effective doses of 8.0 and 8.9 mSv from the CT component for the system I, and 7.8 and 8.7mSv for system II. The corresponding effective doses from the PET component were 4.9 and 5.9 mSv for the system I and II respectively. One evaluation of 105 PET/CT scanners used in 73 institutions in Korea (Kwon et al [36]) estimated the average effective dose from FDG to be 5.89 ± 1.46 mSv and 6.26 ± 3.06 mSv from CT. The researchers observed that the total radiation dose was reduced with scanners equipped with image – enhancing algorithms [36].

Another study of 35 oncology patients in Thailand found that the average whole-body effective doses from the PET and CT were 4.40 ± 0.61 and 14.45 ± 2.82 mSv respectively, for the same type of examinations resulting in the total patient dose of 18.85 mSv [37]. Kaushik et al [38] reported that the total effective dose from a typical protocol of whole-body ^{18}F -FDG PET/CT examination was 14.4 mSv for females and 11.8 mSv for male patients. They indicate that the estimated doses were approximately 5-8 times higher than the background radiation dose.

2.6 Role of ^{18}F -FDG-PET/CT imaging in TB diagnosis

The contribution of Positron emission tomography (PET) integrated with computed tomography (CT) to the diagnosis of fever, cough, hemoptysis, appetite and/or weight loss, differentiation of malignant from benign lesions, and assessing therapy response in many infectious and inflammatory conditions of unknown origin is widely reported [39,40]. The main strength of this non-invasive method of imaging lies in its ability to detect primary and metastatic disease deep within the body and conduct longitudinal assessment overtime by means of a whole-body survey with a single injection of a given amount of a radiotracer, such as $2\text{-}^{18}\text{F}$ -FDG fluoro-deoxy-glucose [26,39].

^{18}F -FDG accumulates in inflammatory cells such as neutrophils, activated macrophages, and lymphocytes at the site of inflammation or infection [41], as a result of the respiratory burst that occurs with infection. Consequently, the uptake is observed in both Pulmonary and Extra-pulmonary TB and other TB-related lesions [40]. For instance, in a study by Goo et al [42] involving 10 consecutive patients suffering from histopathologically proved active pulmonary TB at a South Korean hospital, 9 (90%) tuberculomas showed FDG uptake at PET, with a maximum standardized uptake value (SUVmax), the regional radioactivity concentration divided by the total injected dose and adjusted to the patient weight [43] above the threshold of 2.5 at 4.2 ± 2.2 SD.

Moreover, as a decrease in the SUVmax correlates with response to treatment, ^{18}F -FDG-PET has been shown to be very useful in monitoring and guiding the duration of antimicrobial therapy, especially in patients with multi-drug resistant (MDR)-TB where second-line drugs are less efficacious and definitive treatment duration is not known [44-47]. This was

demonstrated in a study by Martinez et al [48], where a 31% median percentage decrease in SUVmax was observed in 19 out of 21 consecutive HIV negative TB patients at one month of therapy. In a separate study of a 52-year-old woman with stage 3B cervical squamous cell carcinoma involving para-aortic lymph nodes, the calculated standardized uptake value (SUV) of the mediastinal nodes was 5.5. Follow-up PET/ CT performed at 24 weeks after commencement of treatment revealed smaller mediastinal lymph nodes and decreased SUV (1.8) [47]. Other studies by Park et al [49] and Chen et al [50] also revealed patients remaining free of TB months after treatment.

It is also reported that ^{18}F -FDG-PET/CT is able to differentiate old or inactive sequellar TB from that in the latent or active stage of infection, particularly in patients with radiological findings alone, as the high ^{18}F -FDG uptake in a patient with TB represent an active disease or a host immune system activity that will eventually prevail [44,49]. Kim et al [51] evaluated the role of ^{18}F -FDG PET/CT imaging in the differentiation of areas of active TB from the old or inactive disease in 25 consecutive pulmonary tuberculoma patients. The study found significantly higher maximal SUVmax values in patients with active rather than inactive tuberculoma, with early and delayed (60 and 120-minutes post injection) SUVmax values of (active = 2.3 ± 0.75 , inactive = 0.79 ± 0.15 and active 2.48 ± 0.79 , inactive = 0.75 ± 0.13) respectively. Soussan et al [45] were able to describe two distinct patterns of pulmonary TB: (1) the lung pattern, related to a restricted and slight hyper-metabolic infection, with ^{18}F -FDG uptake in areas of lung consolidation and (2) the lymphatic pattern, related to a systemic and intense infection, with more enlarged and ^{18}F -FDG-avid hilar and mediastinal lymph nodes using the PET/CT imaging.

The most promising role of FDG-PET/CT is probably in the monitoring of treatment response, especially in extra-pulmonary TB where obtaining tissue/fluid for analysis is not always possible or may be invasive [39]. PET/CT is important in detecting subsets (<1%)

of the *Mycobacterium tuberculosis* (Mtb) that may emerge within the bacterial population during sub-optimal treatment with inadvertent monotherapy. These subsets reflect naturally occurring drug-resistant mutants, which other new and traditional diagnostics methods such as interferon gamma release assay (IGRA), urine lipoarabinomannan (LAM) testing including the liquid culture has failed to detect [39]. The early detection of these subsets in the course of treatment enables timely change to appropriate therapy.

2.7 The significance of CT in FDG-PET/CT imaging

Over the past years, ¹⁸fluorodeoxyglucose (18F-FDG)-positron emission tomography (PET) has proved to be a valuable imaging technique for diagnosing many cancer diseases, accurate determination of the tumor size, delineation of the adjacent structures, the involvement of hilar and mediastinal lymph nodes and the detection of distant metastases [52,53]. Its main limitation, however, includes the relative lack of spatial resolution, the low contrast between different tissues, and blurring due to motion and partial volume effects in small foci [52]. Furthermore, tumor tissues like microscopic tumor deposits (tumor nodules in the lymphatic drainage bed of the (primary) tumor) and biologically weak tumors, such as bronchoalveolar cell carcinoma, carcinoid tumors, often show little or no FDG uptake [54].

This limitation and the need to be familiar with the normal physiologic distribution of the tracer and frequently encountered physiologic variants, to accurately interpret the ¹⁸F-FDG findings [54], has necessitated the concept of the integrated positron emission tomography (PET) and computed tomography (CT) system. The CT component of the system provides very detailed imaging information of regions identified on the PET tracer uptake images [52]. This shift to dual-modality imaging has been shown to increase the diagnostic accuracy of FDG-PET scans from 91% to 98% [29]. In a study by Hany et al [55], 21% of all lesions were

classified as undecided with the PET alone. However, using a low-dose CT (10–40 mA) for image co-registration, an additional 7% of all lesions were correctly classified. The number of undecided lesions was reduced to 12% with an 80-mA CT. Beyer et al [28] tested the diagnostic effectiveness of the combined PET/CT imaging in 3 representative case studies of oncology patients. A 78-y-old man with squamous cell carcinoma of the lung, a 69-y-old man with diagnosed primary oesophageal adenocarcinoma, and a 38-y-old woman with a history of unresectable pancreatic cancer. The study found that the fused PET/CT image enabled precise localization of the tumors compared with separate CT and PET images.

The major benefit of CT in integrated PET/CT imaging lies perhaps in the determination of the stage of an unexpected lesion [56]. Whole-body FDG–PET scans often provides imprecise information on the exact location of focal abnormalities because the ^{18}F -FDG tracer is also taken up by muscles and inflammatory processes [57]. However, PET/CT increases specificity and sensitivity in the detection of cancer involvement, which is essential for accurate staging when compared with one of the two imaging modalities used alone, owing to the fusion of the functional information provided by PET with the anatomic information from CT [53]. Cerfolio et al [58] in their study to evaluate the accuracy of staging using integrated PET/CT compared with dedicated PET alone, observed the PET/CT is better predictor than the PET alone for all stages of cancer: Stage I (52% versus 33%) and stage II (70% versus 36%). Other research studies by De Wever et al [52], De Wever et al [56] and Lardinois et al [57] have also shown that the integrated PET/CT technique significantly increases the accuracy of tumour staging when compared with CT and PET alone.

Another more technical, advantage of the CT data of combined PET/CT is that it serves as attenuation map for the PET image attenuation (and scatter) correction [26, 59]. Conventional PET scans require a lengthy transmission scan (set of corresponding images) for attenuation correction of the emission data when a quantitative assessment of the FDG

metabolism is needed. The acquisition of the transmission scan with an external high-energy photon source (germanium-68 or caesium-137) prior or after tracer injection, increases the total scanning time by 50% and also results in data with relatively high noise level [27, 59]. However, the CT-based attenuation correction significantly reduces the overall whole-body scan time by at least 30% – 40%, lower the noise emission scan and improves the precision of the attenuation correction factors [27-29], ultimately leading to a higher patient throughput with less discomfort.

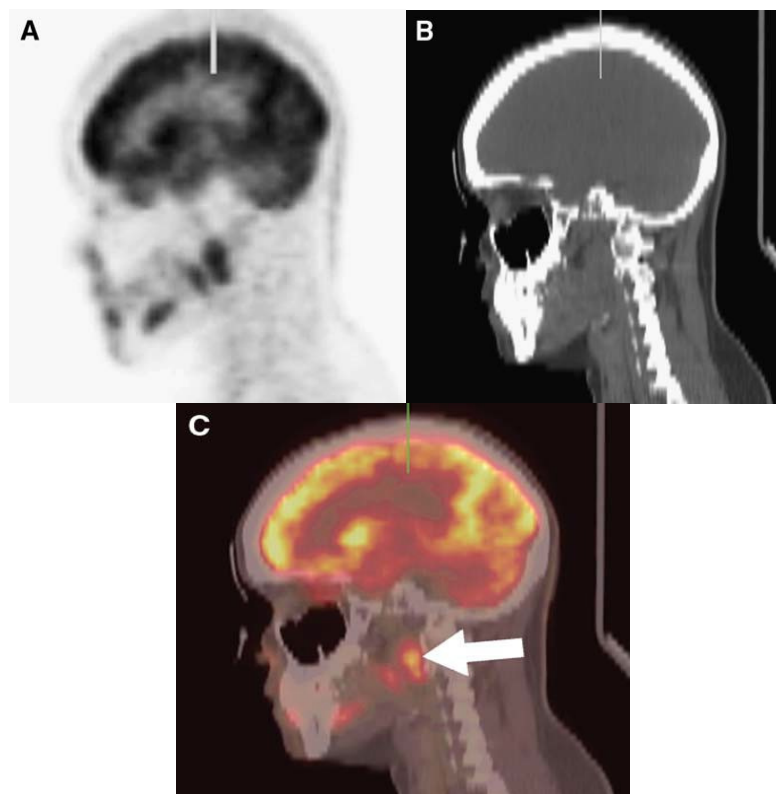


Figure 2.7: Tumor localization and image alignment with a PET/CT scanner: **A** and **B** is the sagittal PET and reformatted CT images of the head. **C** is the combined PET/CT image showing tumor localization in the right retropharyngeal space (arrow) [26]

2.8 Factors affecting patient dose in computed tomography

Recent rapid technological advances in CT scans are intended to minimize the dose received by the patient while accelerating the process of data acquisition and image quality. According to the ALARA principle, the radiation dose must always be reduced to a level where the image quality is still reasonably adequate for diagnostic purposes [31, 60].

The patient dose from a specific CT acquisition is dependent on two factors: Intrinsic and extrinsic factors. Intrinsic factors are related to the geometry and design of the scanner (tube, focus, collimator, filtration, detector design, etc.). Extrinsic factors are parameters such as the maximum tube voltage (kVp), tube current (mA), rotation or exposure time, scan pitch, modulated by the technologist to obtain the desired image quality [14,23]. This section focuses on how these factors affect the radiation dose as well as the image quality.

2.8.1 Scanner geometry

The distance between the x-ray source (focal spot in the tube) and the center of rotation (isocenter) of a scanner is determined primarily by the scanner geometry. All CT scanners possess either a long or short geometric configurations which following the inverse square law, radiation intensity varies with the inverse of the squared distance between source and patient affects the dose received. Explicitly, a short-geometry scanner, if all other scanning parameters are identical, including the radiation beam profile will yield more interaction of radiation with the patient than a long-geometry scanner. This disparity in geometry between different scanner models even from the same manufacturer underscores the fact that

protocols are scanner specific and should not be transferred from one scanner to another without specific investigation [14, 61].

2.8.2 Beam collimation

The collimation of the x-ray beam defines the RPW (nominal x-ray beam width seen at the isocenter) which determine the magnitude and distribution of the absorbed radiation dose. It is equivalent to the nominal section thickness for a single-detector CT but depends on the CT mode and table speed in multidetector CT scanners. Because the x-ray beam is always slightly wider than the beam collimation (number of data channels being used in the Z dimension of the detector) in multi-slice scanners, some amount of the beam is incident beyond the active detector area owing to penumbra effect (also referred to as “overbeaming”) [61, 62].

Generally, wider beam collimation settings result in a more dose-efficient examination, than a narrow collimation, as overbeaming constitutes a smaller proportion of the detected x-ray beam. However, depending on the scanner model, wide collimation means that small abnormalities might be missed or limits the width of the thinnest sections that can be reconstructed. Therefore, the need for a narrow beam collimation to obtain thinner slice widths to improve spatial resolution in the z-axis must be balanced against the associated increased radiation dose [14, 63].

2.8.3 Pitch factor

Pitch is defined as the ratio of table feed per gantry rotation to the nominal collimated width of the x-ray beam. It is a notable adjustable parameter that can affect both the radiation dose and image quality. This is primarily because of the direct relationship between the pitch, beam collimation and table speed for multi-detector scanners [14, 64]. An increase in pitch increases the relative speed of moving the body in the x-ray beam and, consequently, reduces the radiation dose. Paterson et al [65] reported that increasing the pitch of a single-detector scanner with a 1.0 sec gantry rotation cycle from 1.0 to 1.5 leads to a 33% decrease in radiation dose. The radiation dose saving was as high as 50% by changing simply the pitch value from 1.0 to 2.0.

Although scans obtained at a higher pitch, if all other factors are unchanged, will result in lower radiation doses compared with those obtained at a lower pitch, this does not apply to multislice helical CT system using the effective mAs or mAs per slice setting. In such systems, the effect of pitch on dose is negated by a proportional increase in tube current to maintain similar image noise [63, 66]. Additionally, the high-pitch technique has some potential drawbacks that include interpolation artifacts, degradation of the section-sensitivity profile and decrease in spatial resolution that can compromise the image quality [14,63,64]. Hence, CT users should monitor other parameters when changing pitch for safe imaging.

2.8.4 X-ray beam-shaping filters

X-ray beam filters are physical objects positioned between the x-ray source and the patient to attenuate and ‘harden’ the beam spectra so that the x-ray beam is hard enough to efficiently

penetrate the patient while providing sufficient contrast information [67]. This is achieved by cutting off low-energy components of the spectra that constitute absorbed radiation that never reaches the detectors and thus does not contribute to the image [14,64]. Some filters (e.g., bowtie) are specially designed to reduce the incident x-ray intensity in the peripheral region of the patient where attenuation is lowest. A bow-tie filter can minimize the skin dose by 50% compared with a flat filter [62]. Similarly, Itoh et al [68] noted a 17% reduction in radiation exposure and a 9% decrease in image noise with an aluminum filter (5.8mm thick at the center) in contrast to a conventional filter.

2.8.5 Tube current (mA) and tube current-time product (mAs)

The tube current-rotation time product (mAs) determines the photon fluence, which is the number of photons passing through an imaginary sphere, of cross-sectional area $1m^2$ on the surface of the patient during a radiographic procedure [14]. Hence, the patient dose is directly proportional to the tube load (the product of tube current and the exposure time per rotation, mAs) when all other factors are held constant [63, 69]. A 50 % reduction in tube load reduces the radiation dose by half, but also increases the noise level by a factor of $\sqrt{2}$, thus degrades image quality [14, 31].

Determination of an adequate mA level can be performed using the recently available tube-current modulation technique known as automatic exposure control (AEC). This computer software automatically modulates the tube current to accommodate differences in attenuation due to patient anatomy, shape, and size. The tube current is modulated either as a function of projection angle (angular modulation), longitudinal location along the patients (z-axis modulation) or both [63, 67]. The goal of AEC is to use the optimal radiation level for

any patient to achieve adequate image quality for a given diagnostic task. It is, however, a fundamental responsibility of the CT operator to define a minimum acceptable image quality depending on the specific vendor and system.

2.8.6 Tube Potential (kVp)

This is probably the most important determinant of the patient dose from a CT procedure, because the incident x-ray beam energy primarily depends on the selected tube voltage [14, 70]. Unlike the tube current time product (mAs), which have a linear and relatively predictable effect on image noise and contrast-to-noise ratios, variation in kVp, causes a nonlinear, exponential change in radiation dose and image noise, often necessitating a concomitant adjustment in mAs to preserve image quality [31, 63]. The radiation dose changes approximately with the square of the tube voltage while the image noise is inversely proportional to the change in tube voltage [14, 64]. Therefore, for a given diagnostic task and clinical application, the decisions to decrease the tube potential to reduce radiation dose must be made taking into account the image quality, as a result of the complex relationship between tissue contrast, image noise, and radiation dose that is highly dependent on the patient size.

2.8.7 Scan length

The length of a scan is directly related to the total radiation dose delivered to the patient [67, 70]. Radiation dose increases linearly with increase in the anatomic region scanned due to the exposure of additional tissues and organs [23]. It is important to limit the scan

range to include only the clinical region of interest, particularly when imaging structures such as the heart, for which an increased scan range is unnecessary. Patel et al [71] found that using a small scan range (from the top of the aortic arch to the bottom of the heart) in CT pulmonary angiographic studies can allow diagnosis of pulmonary embolism without any loss of sensitivity but with a reduction in radiation dose of 48%.

2.9 Radiation Protection Principles

The increased awareness of the risk of exposure to ionizing radiation has resulted in efforts to minimize radiation dose incurred during x-ray and nuclear medical imaging tests [34]. In order to ensure judicious use of ionizing radiation with a view to maximize the benefits and minimize the risk, three main principles have been set out in radiation protection system: the ethical justification of an examination, the choice of equipment and procedural optimization and finally, the consideration of diagnostic reference levels (DRLs) [72].

a. Justification :All medical practices that imply patient exposures to ionizing radiation must be justified. The concept of justification means that the benefits from the diagnostic procedure to the exposed individual or to society balance the detriment it causes. It suggests that a specified procedure must be deemed fit to improve diagnosis or treatment or provide necessary information about the exposed individuals. Additionally, all other techniques that can provide the same diagnostic value with probably less dose must be considered before exposure [73].

b. Optimization :Optimization requires that an acceptable balance is achieved between image quality and patient dose, taking social and economic factors into account. This requirement consists that the likelihood of incurring exposures, the number of people exposed

and the magnitude of individual exposure follows the ALARA principle [73, 74]. The basic aim of optimization in radioprotection is to adjust the protection measures for a source of radiation to be commensurate with the diagnostic task at hand.

c. Diagnostic reference levels :The diagnostic reference level (DRL) applies to medical practices in planned exposure conditions to help ensure no individual is exposed to an unacceptable radiation risk level. DRLs” means dose levels in radiological practices or, in nuclear medicine, levels of administered activity, for typical examinations when good and normal practice regarding diagnostic and technical performance is applied [75]. Though is not expected to be exceeded, DRLs values are not fixed in stone and should be applied with flexibility to allow higher doses when indicated by sound clinical judgement [73]. The CT and PET/CT technology imaging has a significant contribution in the ionizing radiation population exposure, with a resultant increased risk of cancer [76]. In this light, these radiation protection principles are highly recommended to avoid unnecessary collective effective dose.

Bibliography

- [1] Khan F.M., (1994) “The physics of radiation therapy”, second edition, Lippincott Williams & Wilkins, Philadelphia, USA.
- [2] Canadian Nuclear Safety Commission (CNSC, 2012). Introduction to radiation. ISBN 978-1-100-21572-3.
- [3] <https://www.epa.gov/radiation/radiation-basics>. accessed 02 March 2018.
- [4] International Atomic Energy Agency (IAEA) (2014) Diagnostic Radiology Physics: A Handbook for Teachers and Students. ISBN 978–92–131010–1. STI/PUB/1564 Vienna.
- [5] Borek C., (1993) Molecular mechanisms in cancer induction and prevention. Environ Health Perspect. 101:237-245.
- [6] Kwan-Hoong Ng (2003) Non-ionizing radiations–sources, biological effects, emissions and exposures Proceedings of the International Conference on Non-Ionizing Radiation (ICNIR), UNITEN.
- [7] Nunes ATC., (2011) Dose Optimization in CT, in Nuclear Medicine and in PET-CT procedures, Msc thesis, University of Coimbra, Portugal.

- [8] Seibert, J.A. and J.M. Boone (2005), X-ray imaging physics for nuclear medicine technologists. Part 2: X-ray interactions and image formation. *J Nucl Med Technol.* 33(1): p. 3-18.
- [9] Thompson C.M. (2015) The Utility of Patient-Specific CT Dose Estimation Maps, PhD Thesis, Cleveland State University, Ohio, United States.
- [10] International Atomic Energy Agency (IAEA) (2004). Radiation, people and environment. (Radiation waste safety). IAEA/PVA.75/04-00391, IAEA publication, Austria.
- [11] Schmid E., Schrader T (2007) Different biological effectiveness of ionizing and non-ionizing radiations in mammalian cells. *Adv. Radio Sci.*, 5, 1–4.
- [12] Elgazzar A.H., Kazem N. (2006) Biological Effects of Ionizing Radiation. In: Elgazzar A.H. (eds) *The Pathophysiologic Basis of Nuclear Medicine*. pp 540-548. Springer, Berlin, Heidelberg
- [13] <https://training.fema.gov/emiweb/is/is302/ssmod02sg.pdf>. accessed 08 March 2018.
- [14] Kalra MK, Maher MM, Toth TL, Hamberg LM, Blake MA, Shepard JA, Saini S. (2004) Strategies for CT radiation dose optimization. *Radiology.* 230:619-628
- [15] ICRP (1991) The 1990 Recommendations of the International Commission on Radiological Protection. ICRP publication 60 *Ann ICRP* 1991, 21,(1-3)
- [16] Lototska O.V (2016) Ionizing radiation as a factor in environmental and industrial hazard. The problem of environmental contamination with radionuclides. accessed 06 February 2018
- [17] ICRP (2007) The 2007 Recommendations of the International Commission on Radiological Protection. ICRP publication 103 *Ann ICRP* 2007, 37, (2-4)

- [18] Desouky O., Nan Ding N., Zhou G (2015) Targeted and non-targeted effects of ionizing radiation. *Journal of Radiation Research and Applied Sciences* 8(2)247-254.
- [19] Saha, G. B., (2013) *Radiation biology in physics and radiobiology of nuclear medicine*. Springer Science Business Media, New York.
- [20] Koturbash I., Kutanzi K., Hendrickson K., Rodriguez-Juarez R., Kogosov D., Kovalchuk O. (2008) Radiation-induced bystander effects in vivo are sex specific. *Mutation Research* 642 (1-2), 28-36.
- [21] Hall, E.J., Giaccia, A.J. (2011) *Radiobiology for the radiologist*. (7th ed.), Lippincott Williams & Wilkins, Philadelphia
- [22] Byrd D.W. (2014) *Tube Current Modulated Computed Tomography Effective Dose and Size Specific Organ Dose Estimates with Impact: Total Scan versus Slice By Slice Parameters for Urogram Protocols*, MSc Thesis, Louisiana State University Baton Rouge, USA.
- [23] Peter Hogg, Giorgio Testanera (2010). *Principles and Practice of PET/CT, Part 1. A Technologist's Guide*. European Association of Nuclear Medicine, ISBN: 978-3-902785-00-8
- [24] National Research Council and Institute of Medicine Committee on the Mathematics and Physics of Emerging Dynamic Biomedical Imaging. Washington (DC): National Academies Press (US); 1996.
- [25] Marcus Söderberg (2008) *Automatic exposure control in CT: an investigation between different manufacturers considering radiation dose and image quality*, Msc Thesis, Medical Radiation Physics Clinical Sciences, Lund University.

- [26] Thomas Beyer, Gerald Antoch, Stefan Muller, Thomas Egelhof, Freudenberg Lutz S., Jorg Debatin, et al. (2004) Acquisition Protocol Considerations for Combined PET/CT Imaging. *J Nucl Med* 45:25S-35S
- [27] Alessio A M., Paul Kinahan E, Cheng PM, Hubert V, Karp JS(2004) PET/CT scanner instrumentation, challenges, and solutions. *Radiol Clin N Am* 42 1017 – 1032
- [28] Thomas Beyer, Townsend DW, Brun T, Paul Kinahan E, Martin Charron, Raymond Roddy, et al.(2000) A combined PET/CT scanner for clinical oncology. *J Nucl Med* 41:1369 – 1379
- [29] Sureshbabu W, Mawlawi O (2005) PET/CT Imaging Artifacts. *J Nucl Med Technol.* 33:156 – 161
- [30] <https://www.radiologycafe.com/radiology-trainees/frcr-physics-notes/pet-imaging>. accessed 12 March 2018
- [31] Mattsson S, Söderberg M. (2011) Radiation dose management in CT, SPECT/CT and PET/CT techniques. *Radiat Prot Dosimetry.* 147(1-2):13-21
- [32] Huang, B., Law, M.W., Khong, P.L., (2009) Whole-body PET/CT scanning: estimation of radiation dose and cancer risk. *Radiology* 251, 166–174.
- [33] Brix G, Lechel U, Glatting G, Ziegler SI, Münzing W, Müller SP, Beyer T. (2005) Radiation exposure of patients undergoing whole-body dual-modality 18F-FDG PET/CT examinations. *J Nucl Med* 46(4):608-13.
- [34] Quinn B, Dauer Z, Pandit-Taskar N, Schoder H, Dauer LT. (2016) Radiation dosimetry of 18F-FDG PET/CT: incorporating exam-specific parameters in dose estimates. *BMC Medical Imaging* 16:41

- [35] Avramova-Cholakova S, Ivanova S, Petrova E, Garcheva M, Vassileva J.(2015) Patient doses from PET-CT procedures. *Radiat Prot Dosimetry*. 165(1-4):430-3
- [36] Kwon HW, Kim JP, Lee HJ, Paeng JC, Lee JS, Cheon GJ, Lee DS, June-Key C, and Kang KW (2016) Radiation Dose from Whole-Body F-18 Fluorodeoxyglucose Positron Emission Tomography/Computed Tomography: Nationwide Survey in Korea. *J Korean Med Sci* 31: S69-74
- [37] Khamwan K, Krisanachinda A and Pasawang P. (2010) The determination of patient dose from 18F-FDG PET/CT examination. *Radiation Protection Dosimetry* 141(1): 50–55
- [38] Kaushik A., Jaimini A., Tripathi M., D’Souza M., Sharma R., Mishra AK., Mondal A. and Dwarakanath BS.(2013) Estimation of patient dose in 18F-FDG and 18F-FDOPA PET/CT examinations. *J. Can. Res.Ther.* 9(3): 477–483
- [39] Ankrah AO, van der Werf TS, de Vries EF, Dierckx RA, Sathekge MM, Andor Glaudemans AW (2016). PET/CT imaging of Mycobacterium tuberculosis infection *Clin Transl Imaging* 4:131-144
- [40] Skoura E, Zumla A, and Bomanji J (2015) Imaging in tuberculosis, *International Journal of Infectious Diseases* 32: 87-93
- [41] Jones HA, Clark RJ, Rhodes CG, Schofield JB, Krausz T, Haslett C (1994) In vivo measurement of neutrophil activity in experimental lung inflammation. *Am J Respir Crit Care Med* 149:1635–9
- [42] Goo JM, Im JG, Do KH, Yeo JS, Seo JB, Kim HY, and Chung JK (2000): Pulmonary tuberculoma evaluated by means of FDG PET: findings in 10 cases. *Radiology* 216:117–121.

- [43] Hara T, Kosaka N, Suzuki T, Kudo K, Niino H (2003) Uptake rates of 18-Fluorodeoxyglucose and 11C-choline in lung cancer and pulmonary tuberculosis: a positron emission tomography study. *Chest* 124:893–901
- [44] Heysell SK, Thomas TA, Sifri CD, Rehm PK and Houpt ER(2013) 18-fluorodeoxyglucose positron emission tomography for tuberculosis diagnosis and management: a case series *BMC Pulmonary Medicine* 13:14
- [45] Soussan M, Brillet PY, Mekinian A, Khafagy A, Nicolas P, Vessieres A, et al (2012) Patterns of pulmonary tuberculosis on FDG-PET/CT. *Eur J Radiol* 81:2872–6.
- [46] Gandhi NR, Nunn P, Dheda K, Schaaf HS, Zignol M, van Soolingen D et al.,(2010) Multidrug-resistant and extensively drug-resistant tuberculosis: a threat to global control of tuberculosis. *Lancet*, 375:1830–1843
- [47] Hofmeyr A, Eddie Lau WF, Slavin MA (2007) Mycobacterium tuberculosis infection in patients with cancer, the role of 18-fluorodeoxyglucose positron emission tomography for diagnosis and monitoring disease response. *Tuberculosis* 87(5):459–463
- [48] Martinez V, Castilla-Lievre MA, Guillet-Caruba C, Grenier G, Fior R, Desarnaud S et. al., (2012) (18) F-FDG PET/CT in tuberculosis: an early non-invasive marker of therapeutic response. *Int J Tuberc Lung Dis*, 16(9):1180–1185
- [49] Park IN, Ryu JS, Shim TS (2008) Evaluation of therapeutic response of tuberculoma using F-18 FDG positron emission tomography *Clin Nucl Med* 33(1):1–3
- [50] Chen RY, Dodd LE, Lee M, Paripati P, Hammoud DA, Mountz JM et al (2014) PET/CT imaging correlates with treatment outcome in patients with multidrug-resistant tuberculosis. *Sci Transl Med* 6(256):265ra166.

- [51] Kim IJ, Lee JS, Kim SJ, Kim YK, Jeong YJ, Jun S et al (2008) Double phase 18 F-FDG PET-CT for determination of pulmonary tuberculoma activity. *Eur J Nucl Med Mol Imaging* 35:808–814
- [52] De Wever W, Ceyssens S, Mortelmans L, Stroobants S, Marchal G, Bogaert J, et al. (2007) Additional value of PET-CT in the staging of lung cancer: comparison with CT alone, PET alone and visual correlation of PET and CT. *Eur Radiol*, 17: 23–32.
- [53] De Wever W, Stroobants S, Coolen J, and Verschakelen J.A (2009) Integrated PET/CT in the staging of non-small cell lung cancer: technical aspects and clinical integration. *Eur Respir J*, 33: 201–212
- [54] Abouzied MM, Crawford ES, Nabi HA (2005) 18F-FDG imaging: pitfalls and artifacts. *J Nucl Med Technol* 33(3):145–155
- [55] Hany TF, Steinert HC, Goerres GW, Buck A, von Schulthess GK (2002) PET diagnostic accuracy: improvement with in-line PET-CT system: initial results. *Radiology*, 225: 575–581.
- [56] De Wever W, Vankan Y, Stroobants S, Verschakelen J. (2007) Detection of extrapulmonary lesions with integrated PET/CT in the staging of lung cancer. *Eur Respir J.*, 29(5):995-1002.
- [57] Lardinois D, Weder W, Hany TF, Kamel EM, Stephan Korom, Burkhardt Seifert, et al. (2003) staging of non-small-cell lung cancer with integrated positron-emission tomography and computed tomography. *N Engl J Med.*, 348: 2500–2507.
- [58] Cerfolio RJ, Ojha B, Bryant AS, Raghuveer V, Mountz JM, Bartolucci AA. (2004) The accuracy of integrated PET-CT compared with dedicated PET alone for the staging of patients with nonsmall cell lung cancer. *Ann Thorac Surg* 78: 1017–1023.

- [59] Schöder H, Erdi YE., Larson SM, Yeung HW (2003) PET/CT: a new imaging technology in nuclear medicine. *Eur J Nucl Med Mol Imaging* 30:1419–1437
- [60] Noor JAE, Normahayu I (2012) An Attempt to Establish National Dose Reference Levels for Head CT-Scan Examinations in Indonesia: Preliminary Results from Malang Hospitals. *International Journal of Engineering & Technology* 12 (6), 109-114
- [61] Hamberg LM, Rhea JT, Hunter GJ, Thrall JH (2003) Multi-detector row CT: radiation dose characteristics. *Radiology* 226(3):762-72
- [62] Toth TL (2002) Dose reduction opportunities for CT scanners. *Pediatr Radiol.* 32: 261–267
- [63] Raman SP, Mahesh M, Blasko RV, Fishman EK (2013) CT scan Parameters and Radiation Dose: Practical Advice for Radiologists. *J Am Coll Radiol.* 10(11):840-846.
- [64] Aweda MA, Arogundade RA (2007) Patient dose reduction methods in computerized tomography procedures: A review *International Journal of Physical Sciences* Vol. 2 (1), pp. 001-009
- [65] Paterson A, Frush DP, Donnelly LF (2001) Helical CT of the Body: Are Settings Adjusted for Paediatric Patients? *AJR Am J Roentgenol.* 176(2):297-301.
- [66] Mahesh M, Scatarige JC, Cooper J, Fishman EK. (2001) Dose and Pitch Relationship for a Particular Multislice CT scanner. *AJR Am J Roentgenol.* 177(6):1273–1275
- [67] Yu L, Liu X, Leng S, Kofler JM, Ramirez-Giraldo JC, Qu M, Christner J, Fletcher JG, and McCollough CH (2009) Radiation dose reduction in computed tomography: techniques and future perspective. *Imaging Med.* 1(1): 65–84

- [68] Itoh S, Koyama S, Ikeda M, Ozaki M, Sawaki A, Iwano S, et al. (2001) Further reduction of radiation dose in helical CT for lung cancer screening using small tube current and a newly designed filter. *J Thorac Imaging* 16:81–88.
- [69] Prasad SR., Wittram C., Shepard JA, McLoud T., Rhea J (2002) Standard-dose and 50%-reduced-dose chest CT: Comparing the effect on image quality. *Am. J. Roentgenol.* 179(2), 461- 465
- [70] Johnson JO, Robins JM. (2012) CT Imaging: Radiation Risk Reduction — Real-Life Experience in a Metropolitan Outpatient Imaging Network. *J Am Coll Radiol.* 9(11):808-813
- [71] Patel H, Coughlin B, LaFrance T, O'Donnell-Moran G (2007) Comparison of Full Chest CTA with Limited CTA and Triple Rule-out CTA for PE Detection and Effective Dose Implications. Radiological Society of North America 2007 Scientific Assembly and Annual Meeting, Chicago, Illinois. (Accessed November 28, 2017)
- [72] ICRP (2007) Recommendations of the International Commission on Radiological Protection ICRP Publication 103 *Ann ICRP* 37: 2-4
- [73] Kyung-Hyun Do (2016) General Principles of Radiation Protection in Fields of Diagnostic Medical Exposure. *J Korean Med Sci* 31(Suppl 1): S6–S9.
- [74] Scientific Committee on Emerging and Newly Identified Health Risks (SCENIHR) (2012). Health effects of security scanners for passenger screening (based on X-ray technology) doi:10.2772/87426
- [75] ICRP (1996) Radiological protection and safety in medicine, A report of the international commission on radiological protection *Ann ICRP* 26:1–47.

- [76] Kim YY, Shin HJ, Kim MJ, Lee MJ (2016) Comparison of effective radiation doses from X-ray, CT, and PET/CT in pediatric patients with neuroblastoma using a dose monitoring program. *Diagn Interv Radiol.* 22(4):390-4.

Chapter 3

RADIATION DOSE AND CANCER RISK ESTIMATES IN HELICAL CT FOR PULMONARY TUBERCULOSIS INFECTIONS

School of Chemistry & Physics, University of KwaZulu-Natal, Pietermaritzburg Campus,
Private Bag X01, Scottsville 3209, South Africa

This chapter is a published journal article that studied how different CTs types affects the absorbed radiation dose and long-term effects (cancer risks) for exposed patients in helical CT for pulmonary tuberculosis infections with same acquisition protocol. ¹

¹B. Adeleye and N. Chetty, 2017. Radiation dose and cancer risk estimates in helical CT for pulmonary tuberculosis infections. *Open Phys.* 15:769–776

3.1 Abstract

The preference for computed tomography (CT) for the clinical assessment of pulmonary tuberculosis (PTB) infections has increased the concern about the potential risk of cancer in exposed patients. In this study, we investigated the correlation between cancer risk and radiation doses from different CT scanners, assuming an equivalent scan protocol. Radiation doses from three 16-slice units were estimated using the CT-Expo dosimetry software version 2.4 and standard CT scan protocol for patients with suspected PTB infections. The lifetime risk of cancer for each scanner was determined using the methodology outlined in the BEIR VII report. Organ doses were significantly different ($P < 0.05$) between the scanners. The calculated effective dose for scanner H2 is 34% and 37% higher than scanners H3 and H1 respectively. A high and statistically significant correlation was observed between estimated lifetime cancer risk for both male ($r^2 = 0.943$, $P < 0.05$) and female patients ($r^2 = 0.989$, $P < 0.05$). The risk variation between the scanners was slightly higher than 2% for all ages but was much smaller for specific ages for male and female patients (0.2% and 0.7%, respectively). These variations provide an indication that the use of a scanner optimizing protocol is imperative.

Keywords: Pulmonary tuberculosis; Computed tomography; Radiation dose; Lifetime attributable risk of cancer

3.2 Introduction

Tuberculosis (TB) is an infection caused by *Mycobacterium tuberculosis* and is one of the leading causes of mortality and morbidity in the world. The World Health Organization (WHO) global tuberculosis report (2014) estimated that 9.0 million people developed TB in 2013, of which 1.5 million died [1]. Pulmonary tuberculosis (PTB), classified as primary and post-primary (reactivation), is considered to be the most infective form of the disease, and it occurs in more than 80% of TB cases [2, 3]. To date, tuberculosis remains endemic in most of the developing countries and countries with high rates of infection with human immunodeficiency virus (HIV), including South Africa. The estimated incidence of undiagnosed active TB infection in South Africa is 450,000 patients [1, 4]. The KwaZulu-Natal province, where HIV infection rates are high, has been the most affected region, accounting for 22% (99,067) of the patients. The WHO report indicates that this rate represents an increase of approximately 400% over the past 15 years [1] and represents the third highest infection rate of any country worldwide after India and China. This high rate is largely attributed to both late and poor diagnosis and leads to delays in the appropriate treatment of infected patients. To date, the mainstay for the diagnosis of adult chest TB is the identification of acid-fast bacilli (AFB) by sputum smear microscopy. However, previous studies have shown that acid-fast bacilli are found in the sputum of a limited number of patients (20% – 55%) with active pulmonary TB [5]. Moreover, smear microscopy results are available within days, while the culture results of *M. tuberculosis* from sputum requires (3 – 8) weeks for results, primarily because of the slow growth of the organism [6]. These limitations have increased the importance of medical imaging as a diagnostic procedure for the evaluation of suspected TB and PTB. Despite the increased doses of radiation compared with radiography and the need for the administration of intravenous contrast agent, CT remains the method of choice for the

diagnosis of primary and post-primary PTB [3, 7]. CT is more sensitive than chest radiography for making the diagnosis and characterizing the cases of both subtle and disseminated parenchymal disease and mediastinal lymphadenopathy that are predominantly situated in peripheral subregions. CT is also more sensitive for the evaluation of cases of tuberculous effusion, emphysema, and bronchopleural fistula that are not evident on plain radiographs[8-12]. The increased use of CT, and in particular helical CT, for higher resolution and higher definition of internal structures for the diagnosis of suspected PTB before treatment, has raised concerns about the radiation dose and associated cancer risk for exposed individuals. Although the risk for the general population is small and non-uniform, a previous study has shown that an increase in the exposure to ionizing radiation potentially increases the risk of cancer [13]. Therefore, considering the increase in TB prevalence in the general population, consequent increase in exposure to ionizing radiation from diagnostic testing, and the use of generic protocols by imaging professional, our study aimed to estimate CT radiation doses with the risk of cancer from different 16-slice models, and investigate their correlation, assuming equivalent scan protocol. It is also anticipated that the study will help to understand the benefits of optimizing protocols for imaging technique.

3.3 Materials and Methods

3.3.1 CT models and protocols

The following 16-detector row scanners based on our survey were included in this study: (i) the Toshiba Aquilion 16 (Toshiba Medical Systems) (ii) the GE LightSpeed 16 (General Electric Medical Systems, Milwaukee, WI) and (iii) the Somatom Sensation 16 (Siemens

Healthcare, Germany). Routine scan protocol for patients with suspected PTB infections in an institution in the KwaZulu-Natal province was followed. Patients were scanned at 120 kVp, using an electrical current (mA) setting adapted to the patient's weight up to a maximum of 200 mA for patients with larger body habitus to ensure proper pathologic findings of structures in the lungs and acceptable diagnostic image quality. Images were reconstructed at a slice thickness of either 3 mm or 5 mm. Although exposure parameters were modified to lower the radiation exposure of patients, the parameters mentioned above represented the standard scanning protocols largely employed. For purposes of privacy protection, the scanners were coded randomly as H1 - H3.

3.3.2 Dose assessment

Organ-specific doses were estimated using the CT-Expo (version 2.4) dosimetry software with adult male phantoms (ADAM; 170-cm height and 70-kg weight) and adult female phantoms (EVA; 160-cm height and 60-kg weight)[14]. CT-Expo is a Microsoft Excel application that allows the computation of age- and sex-specific radiation (organ and effective) doses on the basis of the inputted scanner model, manufacturer, scanning parameters, and scanned area using one of four anthropomorphic mathematical phantoms (ADAM, EVA, CHILD, and BABY) and organ dose data generated by Monte Carlo simulation methods [15, 16]. The mathematical phantoms allowed us to indicate precisely the prescribed anatomical range and obtain more accurate radiation dose estimation for CT examinations as there is no underestimation issue from insufficient voxel images sampling. Simulations were performed in each scanner using the maximum mA and standard scanning parameters settings (Table 3.1), and anatomic regions (Table 3.2). We selected the widest X-ray beam width or maximum available detector channels in each scanner, the rotation time of 1 second, slice thickness of

Table 3.1: Summary of the technical parameters used in three 16- slice computed tomography scanners evaluated in this study.

Scanner	H1	H2	H3
Tube Potential (kV)	120	120	120
Tube Current (mA)	200	200	200
Detectors (mm)	16 x 1.5	16 x 2.0	16 x 1.25
Mode	Helical	Helical	Helical
Beam Collimation	24	32	20
Pitch	1.25	1.437	1.375
Table Feed (TF) (mm/rot)	30.0	46.0	27.5
Slice thickness (mm)	5	5	5
Rotation time (s)	1	1	1

5 mm, and related spiral pitch factor for ease of comparison.

The volume CT dose index (CTDI_{vol}) is a standardized value of the respective radiation output of each scanner measured in a 32-cm diameter acrylic phantom with helical scanning mode. The product of the volume CT dose index (CTDI_{vol}) and the irradiated scan length (L) is the dose-length product (DLP), which represents a measure of the total energy delivered to a patient from a specific CT acquisition. DLPs value for each scanner was averaged over the male and female patient phantoms. The effective dose E was calculated on the basis of tissue weighting factors, as detailed in publication 103 from the International Commission on Radiological Protection (ICRP). CTDI_{vol}, the corresponding value of DLP (in mGycm) and effective dose E were determined using the CT Expo dosimetry software version 2.4[14].

Table 3.2: Anatomical extent of computed tomographic examinations using CT-Expo mathematical phantoms

Anatomical Region	Sex	Start and End Z coordinate (cm)	Scan Length (cm)	Organ Position
Thorax	Male	42 and 69	27	From top liver to below shoulders; Lungs centered at 54 cm
	Female	40 and 65	25	From top liver to below shoulders; Lungs centered at 51 cm, breast at 45 cm

3.3.3 Calculation of the attributable risk of cancer

The lifetime attributable risk (LAR) of cancer incidence, which indicates the risk of developing whole-body or organ-specific cancer for each sex after radiation exposure at a certain age, was estimated using Table 12D-1 of the phase 2 report of the National Academies Committee on the Biological Effects of Ionizing Radiation (BEIR) VII [17]. The LAR was estimated on the basis of protocols employed during the scans and the scanner type. Organ-specific LARs were determined from organ-equivalent doses using a linear no-threshold assumption for the organs specified in the BEIR report. Whole-body LAR was calculated by summation of organ-specific LARs for the various organs and adding a composite equivalent dose for other malignancies not included in the BEIR report. The linear interpolation of the two nearest ages was performed for cases in which organ-specific risk factors for a specific age were not available. The risk estimation method described above has been used in several studies to estimate the cancer risk from CT radiation [18-20].

Statistical analysis

A one-way analysis of variance (ANOVA) was used to determine significant differences in organ doses between the sexes and scanners. The relationship between the estimated cancer risk for male and female patients in all scanners was analyzed by linear regression. All statistical analyses were performed using Origin software version 6.1 [20] and Microsoft Excel 2013 at a significance level of 0.05.

3.4 Results

3.4.1 Organ-specific and effective doses

Table 3.3 shows the estimated equivalent doses in radiosensitive organs with a strong proclivity for carcinogenesis according to the BEIR VII report [17], including directly exposed and adjacent organs for the three 16-slice CT models. Significant differences in radiation doses were observed between the different scanners for male ($P = 0.048$, $F = 2.746$) as well as female patients ($P = 0.035$, $F = 2.989$). Overall, scanner H2 produced the highest doses compared with the other models, especially in organs such as the heart, lungs, and breast for female patients within the field of view. Variability in organ doses was observed, particularly because of differences in detector collimation and pitch ratio, despite the use of equivalent scanning parameters [21]. Effective dose (De) values (calculated on the basis of tissue weighting factors and averaging between patients for each acquisition and scanner type, as detailed in ICRP 103 [22]), were highest for scanner H2 (11.1 mSv), followed by H3 (7.35 mSv), and scanner H1 (7.00 mSv). The $CTDI_{vol}$, which indicates the radiation output, particularly for scanners operating in helical mode, obtained using the selected acquisition parameters

was highest for scanner H2 (16.3 mGy) and lowest for the scanner H1 (12.2 mGy). These observed disparities are likely due to the relationship between CTDI_{vol} and the pitch ratio of different CT models, which affects the X-ray beam width and table feed per gantry rotation in helical scanning [23].

3.4.2 Attributable risk of cancer

The LAR of cancer incidence for each scanner for the ages considered is shown in Figure 3.1 and Figure 3.2. The LAR varied slightly according to a patient's age, sex, and scanner type, and a typically high risk was observed with the scanner H2. For a 20-year-old woman, the LARs of 1 in 106, 1 in 172, and 1 in 170 were associated with scanners H2, H3, and H1 respectively. For a 20-year-old man, the LARs of 1 in 143, 1 in 237, and 1 in 228 were associated with the scanner H2, the H3, and H1, respectively. Pearson correlation and linear regression analysis of estimated risk for the different 16-slice units revealed a high and statistically significant correlation ($r^2 = 0.943$, $P < 0.05$) and ($r^2 = 0.989$, $P < 0.05$) between cancer risk for male and female patients, but a negative correlation between cancer risk and age, indicating a lower risk of cancer for older patients. The negative correlation between cancer risk and age is attributed primarily to the BEIR VII risk models [17] and corresponded to a risk reduction of approximately 63% (73% with the scanner H2) for a 50-year-old male patient and 66% for a 50-year-old female patient, relative to a 15-year-old male and female patient, for all scanners.

The relative variations in the estimated risk between the scanners, calculated as the difference between maximum and minimum values, normalized by the mean, were slightly higher than 2% for all ages but were much smaller for specific ages for both male and female patients

Table 3.3: Estimated dose (mSv) from a single helical CT scan for diagnosis of pulmonary tuberculosis with three 16-slice scanners

Organs	H1		H2		H3	
	Male	Female	Male	Female	Male	Female
Gall bladder	5.2	5.0	11.7	11.9	4.5	4.3
Liver	6.9	6.8	12.1	12.3	6.3	6.0
Colon	0.3	0.3	0.6	0.7	0.2	0.3
Esophagus	18.0	18.3	23.9	24.4	20.6	21.0
Adrenal glands	9.3	8.8	14.1	14.3	7.8	7.1
Breasts	0	19.5	0	25.9	0	22.3
Lungs	18.7	18.6	22.1	22.1	21.2	21.1
Lymph nodes	4.8	4.5	7.0	6.7	5.2	4.8
Stomach	4.6	4.5	9.0	9.0	4.1	3.9
Ovaries	0	0.1	0	0.1	0	0
Skin	4.5	4.8	6.6	7.0	4.9	5.2
Bone surfaces	12.3	12.6	15.5	16.0	13.6	13.9
Spleen	5.8	5.5	11.8	11.7	4.9	4.5
Pancreas	5.2	5.0	11.7	11.9	4.5	4.3
Small intestine	0.2	0.2	0.4	0.5	0.2	0.2
ET tissue	11.2	13.0	15.7	17.1	6.9	8.2
Bone marrow	4.6	4.8	6.6	6.8	5.1	5.3
Heart	16.3	15.8	21.9	21.2	18.5	17.9
Muscle	4.8	4.5	7.0	6.7	5.2	4.8
Thyroid	11.2	13.0	18.7	20.1	6.9	8.2
Thymus	18.0	18.3	23.9	24.4	20.6	21.0
Effective dose	7.0		11.1		7.35	
<i>CTDI_{vol}</i> (mGy)	12.2		16.3		13.7	
DLP(mGycm)	388.5		589		404.5	

(up to 0.2% and 0.7%, respectively). This finding indicates that, despite differences in the scanner models and technologies (pitch and collimation), the correlation between age and cancer risk was similar between the scanners. Overall, the estimated risk in female patients was significantly higher than that in male patients of the same age. Accordingly, the LARs for a 35-year old woman were 0.340%, 0.344%, and 0.546% compared with 0.255%, 0.265%, and 0.421%, respectively, for a 35-year-old man, using scanners H3, H1, and H2, respectively. Tables 3.4 and 3.5 summarize the contribution of organs exposed to the highest radiation to whole-body risk. The estimated LARs in these organs were lower than 0.1% for individuals aged 25 years or older, who represented the majority of patients undergoing CT evaluation for PTB disease.

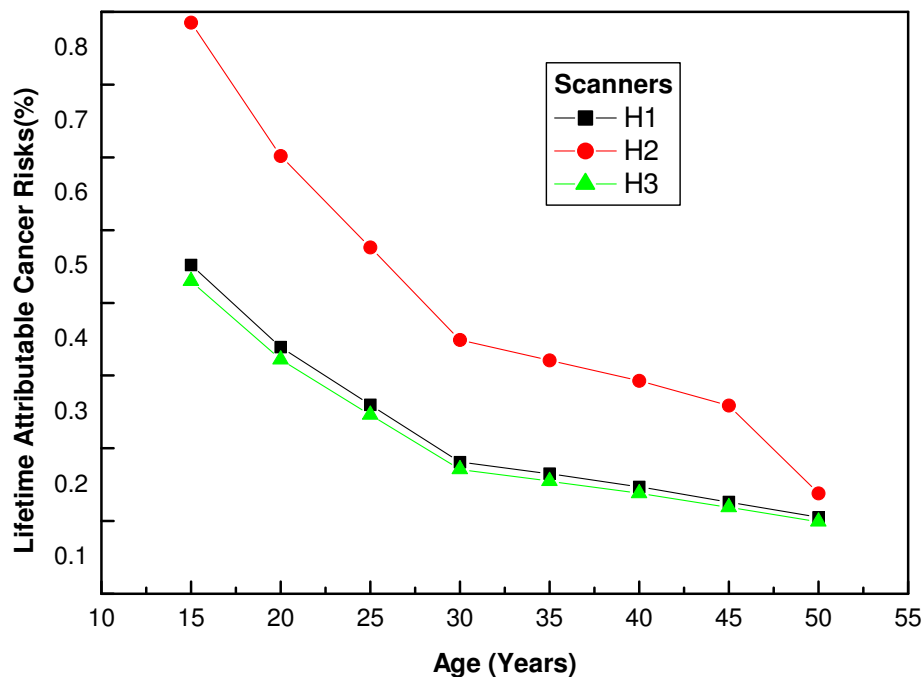


Figure 3.1: Estimated lifetime risk of cancer with respect to age from a single standard computerized tomography dose for diagnosis of pulmonary tuberculosis infections in male patients

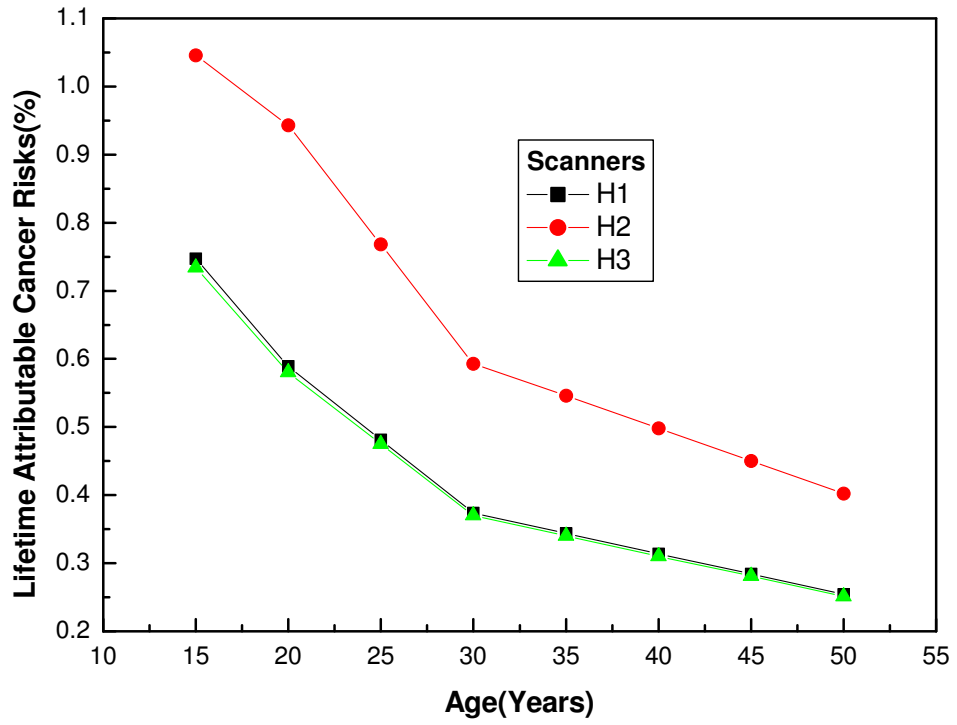


Figure 3.2: Estimated lifetime risk of cancer with respect to age from a single standard computerized tomography dose for diagnosis of pulmonary tuberculosis infections in female patients

Table 3.4: The Contributions of organs exposed to the highest radiation (Breasts and Lungs) for female patients

Age (Years)	LUNGS			BREASTS		
	H1 (%)	H2 (%)	H3 (%)	H1 (%)	H2 (%)	H3 (%)
15	0.0776	0.1047	0.0880	0.1078	0.1432	0.1233
20	0.0644	0.0868	0.0730	0.0836	0.1111	0.0957
25	0.0547	0.0738	0.0620	0.0665	0.0883	0.0760
30	0.0450	0.0607	0.0511	0.0493	0.0655	0.0564
35	0.0448	0.0605	0.0508	0.0384	0.0510	0.0439
40	0.0446	0.0602	0.0506	0.0275	0.0365	0.0314
45	0.0437	0.0590	0.0496	0.0206	0.0273	0.0235
50	0.0428	0.0577	0.0485	0.0136	0.0181	0.0156

Table 3.5: The Contributions of organs exposed to the highest radiation (Lungs) for male patients

Age (Years)	LUNGS		
	H1 (%)	H2 (%)	H3 (%)
15	0.0337	0.0452	0.0382
20	0.0279	0.0374	0.0316
25	0.0237	0.0319	0.0269
30	0.0196	0.0265	0.0224
35	0.0196	0.0264	0.0223
40	0.0195	0.0261	0.0220
45	0.0192	0.0257	0.0217
50	0.0189	0.0254	0.0214

3.5 Discussion

In this study, we estimated the probability of developing cancer from radiation produced by three 16-slice CT scanners used in PTB diagnosis and assuming equivalent scan protocol. A small increase in cancer risk at low doses could result in a significant increase in the number of cases of cancer in a population in which many individuals are exposed to radiation [24]. As expected, critical organs (breast and lungs) along with the esophagus, thymus, bone surfaces, thyroid, and heart, which are in the direct path of X-ray beams, absorbed the greatest amount of radiation. Overall, the doses absorbed by these organs lied within the 10 – 30 mGy range reported by Mettler et al. [25] for organs in the direct path of X-ray beams from CT scans. The comparison of average effective dose (De) values for all scanners indicated that the scanner H2 delivers higher dose respect to the other two scanners, while scanners H3 and H1 deliver about the same dose. However, these results were expected and might be partly explained by technique parameters, such as tube current – time product (mAs) settings, the contrasting scanner geometry of the CT models as well as the correlation between the table feed per 360° rotation of the x-ray tube, beam collimation and pitch factor in helical scanning. For scanner geometry, the relative positions of the x-ray source (focal spot in the tube) and the center of rotation (isocenter) significantly affect the absorbed dose in a patient.

This follows from the inverse square law, radiation intensity varies as the inverse of the squared distance between the radiation source and point of measurement and might explain the slight difference in radiation dose between the scanners H1 and H3 with a focal spot to an isocenter distance of 535 and 541 mm respectively. It is, however, noteworthy that for the scanner H2, despite a longer focal spot to isocenter distance and lowest effective milliamperere-second setting in contrast to other CT models, delivered the highest radiation

dose.

This finding demonstrates the influence of selected scan parameters. While examinations performed at a higher pitch like in the scanner H2 is found to generally reduce radiation exposure [26], the use of effective mAs (mAs/pitch) setting by the scanner means that the effect of high pitch on dose is negated by a proportional increase in tube current to maintain similar image noise thereby increasing radiation dose given the linear relationship between tube current and absorbed dose. A combination of the relatively high electrical current (mA) and tube rotation time (seconds) values used could also explain the high radiation dose observed in some scanners particularly the H2. Patient dose is found to decrease linearly with a reduction in either the tube rotation time (faster gantry rotation) or current [27, 28]. Modification of the tube current-time product (mAs) is essential for reducing radiation dose. If the electrical current is increased the gantry rotation time must be reduced by the same factor to compensate for the increased milliamperere value in order not to increase radiation dose.

OVERRANGING AND OVERBEAMING or penumbra effect are also possible contributors to the high radiation doses. Overbeaming is the excess radiation exposure beyond the collimated beam in the z-direction. OVERRANGING refers to the increase in the dose-length product beyond the volume imaged in helical CT owing to the additional rotations that are required in spiral interpolation algorithms. Both effects depend strongly on beam collimation (the number of data channels multiplied by the effective detector row thickness) and additionally the pitch and scan length for overranging effect [29]. It is noted that the greater the number of detectors the wider the beam width that can be obtained. This is consistent with the results indicated in Table 3.3 where the maximum DLP value was for the scanner H2 at 589 mGycm. Choosing a collimation that is unnecessarily narrow will increase overbeaming but reduce the overranging effect. Conversely, a wider collimation, high pitch, and short

scan length such as in some scanners for this study increases overranging but decrease the overbeaming effect. Therefore to reduce dose a relative adjustment of beam collimation and helical pitch must be made for the patient size and specific clinical problem.

These results highlight the need for caution in transferring scan parameters from one scanner to another and the maintenance of image quality at the lowest radiation dose, depending on scanner characteristics [30]. In general, the effective doses in each scanner were within the range of 4.0 – 18.0 mSv reported in the literature for a full diagnostic helical chest CT examination [25]. However, it is of note that the same effective dose does not correspond to the same cancer risk [31], and this is evidenced by the significantly higher estimated whole-body risk using the scanner H1 compared with the scanner H3, which produced a higher effective dose. The higher estimated risk in female patients than in male patients is attributed to the additional risk of breast cancer together with the increased risk of lung cancer [18, 24]. The overall decrease in LAR with increasing age at exposure (Figure 3.1 and Figure 3.2) is in agreement with the results of other studies [19, 21] where LAR also declined with increasing age. Our cancer risk estimates indicated an elevated risk of breast cancer for women younger than 40 years, followed by lung cancer risk. Similarly, in men, the lungs contributed more to the whole-body cancer risk. The relatively high risk in these organs, particularly breasts in women and lungs in men, of up to 0.1432% and 0.0452%, respectively, for patients aged 15 years, could lead to an increase in these malignancies in the population and constitute a potential public health problem, considering the large number of individuals undergoing CT examinations for PTB diagnosis.

Although the magnitude of LAR estimates reported here appeared to be relatively low for all age categories, these small doses are not necessarily risk-free. There is reasonable epidemiological evidence that organ doses in the range of 5 to 125 mSv results in a small but statistically significant increase in cancer risk [32, 33]. Therefore, the risk of cancer from

radiation exposure should be balanced and weighed against the anticipated benefits obtained from the diagnostic information [34]. Furthermore, exposure should be “as low as reasonably achievable [ALARA principle]. The ALARA principle recommends the optimization of the use of X-rays; therefore, high doses should be avoided because they increase the risk of cancer [32, 35]. Several factors significantly influence the risk of developing cancer following radiation exposure, including genetic effects, age at exposure, sex, fractionated exposure, and protraction of exposure [33]. Therefore, additional studies are required to elucidate the effect of these factors.

This study has some limitations. First, although the dose depended on the scanner manufacturer and model, the CT dose and the risk estimates reported here were based on anthropomorphic mathematical phantoms, which represented reference-sized adults with specific locations for each organ. Therefore, these results might not be applicable to real patients (or might influence the accuracy of the estimates), whose size differed from those of the designated phantoms [21]. Second, some CT acquisition settings, such as exposure scan time relative to the volume of injected contrast media, which is often used to provide optimally enhanced images, were not selected in this study, which simply considered the standard scanning parameters used in routine examinations. In addition, it has to be emphasized that the effects of automatic exposure control (AEC) systems, particularly angular tube current modulation and image quality reference parameters were not analysed within this study because the CT Expo dosimetry software does not account for these options. However, the use of AEC systems depending on the patient size and specified image quality is likely to cause a reduction in radiation dose at different CT models. The magnitude of any such changes has been estimated as being about 11% [21]. Finally, uncertainties are reported to be associated with risk estimation by the BEIR VII report, predicated on the linear no-threshold model. As a result, the emphasis in this study is on the relative differences in estimated absolute

risk between CT systems defining the same scan protocol.

3.6 Conclusions

This study showed significant variations in radiation dose and the lifetime attributable cancer risk between 16-slice scanners used in helical CT scan for pulmonary tuberculosis, using equivalent scan protocol for each model. Although the increase in risk was less than 1% irrespective of the CT scanner producing the highest cancer risk, the related increase in cancer are high enough to warrant reconsideration of means to reduce patient exposure. The need for optimized scanner protocols, that is, exposure protocols that lead to an acceptable image quality for patient-specific indication, based on the individual scanner as opposed to current generic practices with an adverse effect on patient cancer risk are imperative. The aim of this study is not to compare the performance of the different 16-Slice scanners, as this cannot be done based on dosimetric results alone. Each scanner depending on settings such as FOV size, image quality, etc., possesses a wide range of application. Therefore the findings of this work only serve to create awareness for CT practitioners of the consequences of transferring protocols between different scanners.

ETHICAL APPROVAL

This article does not contain any studies with human participants performed by any of the authors.

Acknowledgments

This work was funded by the authors from research allowance given to academic staff of the University of KwaZulu-Natal. No potential conflict of interest is relevant to this article.

Bibliography

- [1] World Health Organization, Global Tuberculosis Report.2014., Available at: <http://www.who.int/tb/publications/global-report/>, Accessed 12. 05. 16.
- [2] De Backer A.I., Mortel K.J., De keulenaer, B.L., Parizel P.M., Tuberculosis: Epidemiology, Manifestations, and the Value of Medical imaging in Diagnosis. JBRBTR., 2006, 89, 243-250.
- [3] Van Dyck P., Vanhoenacker F.M., Van den Brande P.,De Schepper A.M., Imaging of pulmonary tuberculosis.Eur Radiol., 2003, 13, 17711785.
- [4] Churchyard GJ., Mametja LD., Mvusi L., Ndjeka N.,Hesseling AC., Reid A., Babatunde S and Pillay Y. Tuberculosis control in South Africa: Successes, challenges and recommendations. South African Medical Journal,2014, 104(3), 244
- [5] Lee KS, Im JG. CT in adults with tuberculosis of the chest .Characteristic findings and role in Management.AJR, 1995, 164, 13611367
- [6] Foulds J, OBrien R. New tools for the diagnosis of tuberculosis: The perspective of developing countries.Int J Tuberc Lung Dis., 1998, 2,778 83
- [7] Van den Brande P, Vanhoenacker F, Demedts M. Tuberculosis at the beginning of the third millennium: one disease, three epidemics. Eur Radiol., 2003, 13,1767-1770.

- [8] Christophe D., Tania M.M, Valerie B., Jacques de Blic, Natacha S., Denis L. and Scheinmann P . Computed tomography with normal chest radiograph in tuberculous infection. Arch Dis Child, 1993, 69,430-432
- [9] Woodring J.H, Vandiviere H.M., Fried A.M, Dillon M.L, Williams T.D and Melvin IG, Update: the radiographic features of pulmonary tuberculosis. AJR., 1986,146,497506
- [10] McGuinness G, Naidich D.P., Jagirdar J., Leitman B., McCauley DI. High resolution CT findings in miliary lung disease. J Comput Assist Tomogr. 1992,16,384-390
- [11] Hulnick D.H., Naidich D.P., McCauley D.I. Pleural tuberculosis evaluated by computed tomography. Radiology, 1983, 149,759765
- [12] Kim W.S., Moon W.K., Kim I.O., Lee H.J., Im JG, Yeon KM., et.al., Pulmonary tuberculosis in children: evaluation with CT. American Journal of Roentgenology., 1997, 168, 10051009
- [13] Brenner D.J., Hall E.J., Computed tomography an increasing source of radiation exposure. N Engl. J. Med.,2007, 357, 22772284
- [14] Stamm G, Nagel H.D. CT-Expo Version 2.4. A novel tool for dose evaluation in Computed tomography, 2015
- [15] Lopez-Rendon X, Bosmans H, Oyen R, Zanca F. Effective dose and organ doses estimation taking tube current modulation into account with a commercial software package. Eur. Radiol., 2015, 25, 1919-1925
- [16] Kramer R, Zankl M, Williams G, Drexler G. GSF Report,1982, S-88 Part I

- [17] Biological Effects of Ionizing Radiation Committee. Health risks from exposure to low levels of ionizing radiation, BEIR. VII phase 2. Bethesda: National Research Council, National Academy of Science, 2006.
- [18] Einstein A.J., Henzlova M.J, Rajagopalan S. Estimating risk of cancer associated with radiation exposure from 64-slice computed tomography coronary angiography. JAMA, 2007, 298,317323
- [19] Smith-Bindman R, Lipson J., Marcus R., Kim KP., Mahesh M, Gould R., et.al., Radiation dose associated with common computed tomography examinations and the associated lifetime attributable risk of cancer. Arch Intern Med., 2009, 169, 20782086
- [20] Tatum V. T., Geoffrey S., Rajesh S., Estimating the Risk of Cancer Associated With Imaging Related Radiation During Surveillance for Stage I Testicular Cancer Using Computerized Tomography. Journal of Urology, 2009, 181(2), 627-633
- [21] Origin Data Analysis and Graphing Software. Origin Lab Corporation, Northampton, USA.
- [22] Walter H., Kent O.M., Mohammad K. R., Converting Dose-Length Product to Effective Dose at CT. Journal of radiological society of North America, 2008, 248(3) , 995-1003
- [23] ICRP. Recommendations of the International Commission on Radiological Protection ICRP publication 103 Ann ICRP 2007, 37, (24)
- [24] Huda W., Mettler F.A., Volume CT Dose Index and Dose-length Displayed during CT: what good are they? Journal of radiological society of North America, 2011, 258 (1)
- [25] Berrington GA, Mahesh M, Kim KP, Bhargavan M., Lewis R., Mettler F., et.al., Projected cancer risks from computed tomographic scans performed in the United States in 2007. Arch Intern Med. 2009, 169, 20712077.

- [26] Mettler F.A., Huda W., Yoshizumi T.T., Mahesh M. Effective doses in radiology and diagnostic nuclear medicine: A catalog. *Radiology*, 2008, 248(1), 254-263.
- [27] Vade A., Demos T. C., Olson M.C., Subbaiah P., Turbin R.C., Vickery K., et.al, Evaluation of image quality using 1: 1 pitch and 1.5: 1 pitch helical CT in children: a comparative study. *Pediatr Radiol.*1996, 26, 891-893
- [28] Smergel E, Benson D., Radiation dose on pediatric CT: Loosing track of time. *AJR*, 2002, 178(2), 507-508
- [29] Leena H. M., James R. T., George H. J., James T. H., MultiDetector Row CT: Radiation Dose Characteristics. *Radiology*, 2003, 226,762772
- [30] Hans Nagel D., Significance of overbeaming and overranging effects of single- and multi-slice CT scanners, In: *Proceedings of the International Congress on Medical Physics, Nuremburg. 2005*, 50, 395396.
- [31] Madan R.C., Mannudeep K., McCollough C., Nagel HD.,Managing Patient Dose in Multi-Detector Computed Tomography (MDCT) 2006, 32, 219.
- [32] McCollough C.H., Christner J.A., Kofler J.M., How effective is effective dose as a predictor of radiation risk? *AJR Am J Roentgenol*, 2010, 194,890896
- [33] Zanca F, Demeter M, Oyen R, Bosmans H. Excess radiation and organ dose in chest and abdominal CT due to CT acquisition beyond expected anatomical boundaries. *Eur Radiol.*, 2012, 22,779788
- [34] Hricak H., Brenner D.J., Adelstein S.J., Frush D.P., Hall E.J., Howell R.W., et.al., Managing radiation use in medical imaging, a multifaceted challenge *Radiology*, 2011,258,889-905

- [35] Walter Huda. Radiation Doses and Risks in Chest Computed Tomography Examinations. *Atsjournals*, 2007, 4,316-320
- [36] Thomas SL., The ALARA concept in The ALARA Concept in Paediatric CT: Myth or Reality? *Radiology*, 2002,223, 5-6

Chapter 4

RADIATION DOSE FROM ^{18}F -FDG PET/CT PROCEDURES: INFLUENCE OF SPECIFIC CT MODEL AND PROTOCOLS

School of Chemistry & Physics, University of KwaZulu-Natal, Pietermaritzburg Campus,
Private Bag X01, Scottsville 3209, South Africa

This chapter is an accepted manuscript that explored the influence of CT models and protocols on the overall dose from PET/CT procedures. The investigation was carried out for two PET/CT systems and five representative CT protocols. ¹

¹B. Adeleye and N. Chetty. Radiation dose from ^{18}F -FDG PET/CT Procedures: Influence of Specific CT model and Protocols. *Radioprotection*, in press

4.1 Abstract

The increasing use of the integrated ^{18}F -fluorodeoxyglucose (FDG) positron emission tomography/computed tomography (PET/CT) imaging modality in the management of tubercular lesions raises concerns about associated radiation exposure. This work aimed to study the effects of CT model and study protocols on the overall radiation dose from a PET/CT examination. Two PET/CT systems with five representative CT exposure protocols applied for clinical patients in PET/CT imaging following retrospective evaluation were studied. CT doses were calculated using the CT-Expo dosimetry software (version 2.4), while the PET component dose was estimated applying the International Commission on Radiological Protection (ICRP) 106 dose coefficients. The total effective dose ranged from 8.0-24.05 mSv for the system I and 8.35-26.85 mSv for system II, resulting in differences of 4.3%-15% for the Low-dose scan and 4.1%-11% for standard dose scans. The CT component contribution to the total dose was between 32-77% for the system I and 35-79% for system II; however, the contributions were not significantly different ($p > 0.05$) for all protocols. The observed variation in CT contribution represents a requisite pedestal on the need for a nationwide dose assessment for further optimization of the imaging procedure to maximize benefit to patients.

keywords: positron emission tomography- computed tomography imaging; computed tomography scan; radiation exposure; effective dose

4.2 Introduction

The effectiveness of positron emission tomography with ^{18}F -fluoro-deoxy-glucose (^{18}F -FDG) in detecting active tuberculoma and other tuberculosis (TB)-related lesions, assessing the involvement of pulmonary and extra-pulmonary TB and its activity within the body, is well documented [1-4]. The major concern of this non-invasive method of imaging is the additional radiation exposure from CT acquisition together with the internal exposure (γ - ray) from the administered tracer, since FDG-PET scans often require an anatomic imaging study mostly a CT examination, for attenuation correction and optimal tracer uptake interpretation [5-7]. It is known that an ^{18}F -FDG PET/CT scan is accompanied by increased radiation dose capable of enhancing the risk of cancer induction with the CT component contributing up to 81% of the total effective dose [8, 9]. Consequently, modification of the CT imaging parameters has been identified as a significant step to reducing dose to individual patients [10, 11].

South Africa (SA), one of the world's high-burden countries (HBCs) with TB epidemics and the fifth highest number with estimated prevalent (undiagnosed active TB) cases [12, 13] is witnessing a gradual increase in the use of this imaging modality. However, this increasing use of PET/CT in the diagnosis, staging, and assessment of therapy response in infected patients raises the important consideration of the associated radiation dose. The knowledge of dose is essential for clinicians and radiographers in checking standards of good practice as an aid to optimization of patient protection and also determining associated risks so that the diagnostic technique is properly justified [14]. The measure of the potential detriment from a radiographic procedure is best to quantify by the radiation protection quantity, effective dose (ED). ED is not directly measured, but calculated based on equivalent doses to organs and the radiosensitivities of the organs[15,16]. Therefore, assessing the ED of the CT component

of a whole-body PET/CT by experimenting with real subjects are not only dangerous but impossible, and the estimation from the product of the scanner-derived whole-body DLP value and a conversion factor often neglects regional differences when determining CTDI_{vol} and the conversion factor from DLP to ED [17]. Monte Carlo simulation software has become one of the ways of proffering solutions to these problems. The aims of this study were thus to quantify the effects of CT model and exposure protocols on the overall radiation effective dose to patients for commonly performed CT techniques in an ¹⁸F-FDG PET/CT examination, assess if the overall PET/CT dose resulting from the change in CT model and protocols are within acceptable values in literature, and to analyze possible parameters affecting the radiation dose from the CT component. Specifically, comparisons were made between dosimetry results obtained using the CT Expo dosimetry program (version 2.4) from specific CT study parameters during PET/CT acquisition with two different PET/CT systems. The data presented in this study will provide guidance on where efforts on dose reduction will need to be directed to fulfill the requirements of optimization and also serve as a reference for future work.

4.3 MATERIALS AND METHODS

4.3.1 PET/CT System and Protocols

Two 16- slice PET/CT systems from different manufacturers namely the General Electric Healthcare Discovery STE, 16 consisting of a PET scanner with Bismuth germanate oxide (BGO) crystals detector and the Philips Medical Systems Gemini TF 16 with a Lutetium-yttrium oxyorthosilicate (LYSO) crystals detector based PET, denoted as Systems I and II

were considered for this study. Standard Patient preparation included at least 5 h fasting or longer and a serum glucose level of less than 10mmols/l (180 mg/dL) before ^{18}F -FDG injection. PET images were acquired one hour after intravenous ^{18}F -FDG administration typically in three-dimensional mode because of scanner enhanced sensitivity, at 3min per bed position after CT acquisition with the patient positioned so that the PET scan matches the same anatomic extent imaged during the CT acquisition.

The acquisition parameters of the CT protocols in this study (Table 4.1a & 4.1b) were based on what is routinely used for clinical patients in each facility, following retrospective review. Helical transmission CT is performed at photon energy between tube voltages 120–140 kVp, tube current-time was varying by using the automatic exposure control (AEC) technique over the individual patient's anatomy on the basis of a scout view and relative to the prescribed noise index value: 1) a low-dose scan in which the CT component serves as a fast transmission source for attenuation correction and anatomical localization in previously acquired diagnostic CT examinations or 2) a standard radiation dose scan with IV contrast given for attenuation correction and diagnostic purposes. Protocols A and B in each unit, are the low-dose CT scan most frequently performed for PET attenuation correction and anatomic localization. Protocols C, D and E were for diagnostic scans with D and E predominantly for contrast-enhanced studies and patients with larger body habitus wherein the tube current are maximized. The total duration of PET/CT examination was about 25 minutes except in the case of melanoma patients.

Table 4.1: **Standard clinically applied CT exposure parameters used on different PET/CT systems.**

(a)

System I

CT Protocol	Tube Potential (KV)	Tube Current-time (mAs)	Pitch	Acq. Slice thickness (mm)	Beam Collimation (mm)	Table Feed (mm)	Reconstructed slice thickness(mm)
A	120	30	1.75	0.625	10	17.5	3.75
B	120	50	1.75	0.625	10	17.5	3.75
C	120	100	1.75	0.625	10	17.5	3.75
D	120	150	1.75	0.625	10	17.5	3.75
E	140	150	1.75	0.625	10	17.5	3.75

(b)

System II

CT Protocol	Tube Potential (KV)	Tube Current-time (mAs)	Pitch	Acq. Slice thickness (mm)	Beam Collimation (mm)	Table Feed (mm)	Reconstructed slice thickness(mm)
A	120	30	0.75	16 × 1.5	24	18	3
B	120	60	0.75	16 × 1.5	24	18	3
C	120	80	0.75	16 × 1.5	24	18	3
D	120	125	0.75	16 × 1.5	24	18	3
E	140	150	0.75	16 × 1.5	24	18	3

4.3.2 CT dosimetry

The estimation of organ and effective dose (ED) from CT by the CT-Expo dosimetry software (version 2.4, Hannover, Germany) was carried out base on the selection of characteristic CT model, LightSpeed 16, and the Brilliance 16 scanners stored in the software database for each system. The CT Expo Software, an MS Excel application written in visual basic programming permits dose calculations for four gender-specific mathematical phantoms namely

ADAM, EVA, CHILD and BABY [18]. On the account of acquisition protocols presented in (Tabs. 4.1a and 4.1b) with prescribed imaging range (identical for all patients as determined by the ADAM/EVA phantom) covering the entire torso from skull base to the pelvis, embodying common sites of infection such as the cervical, mediastinal, abdominal, and pelvic lymph nodes — (Fig. 4.2) the Effective dose from the CT component was calculated applying the International Commission on Radiological Protection (ICRP) Publication 103 [19] tissue weighting factors.

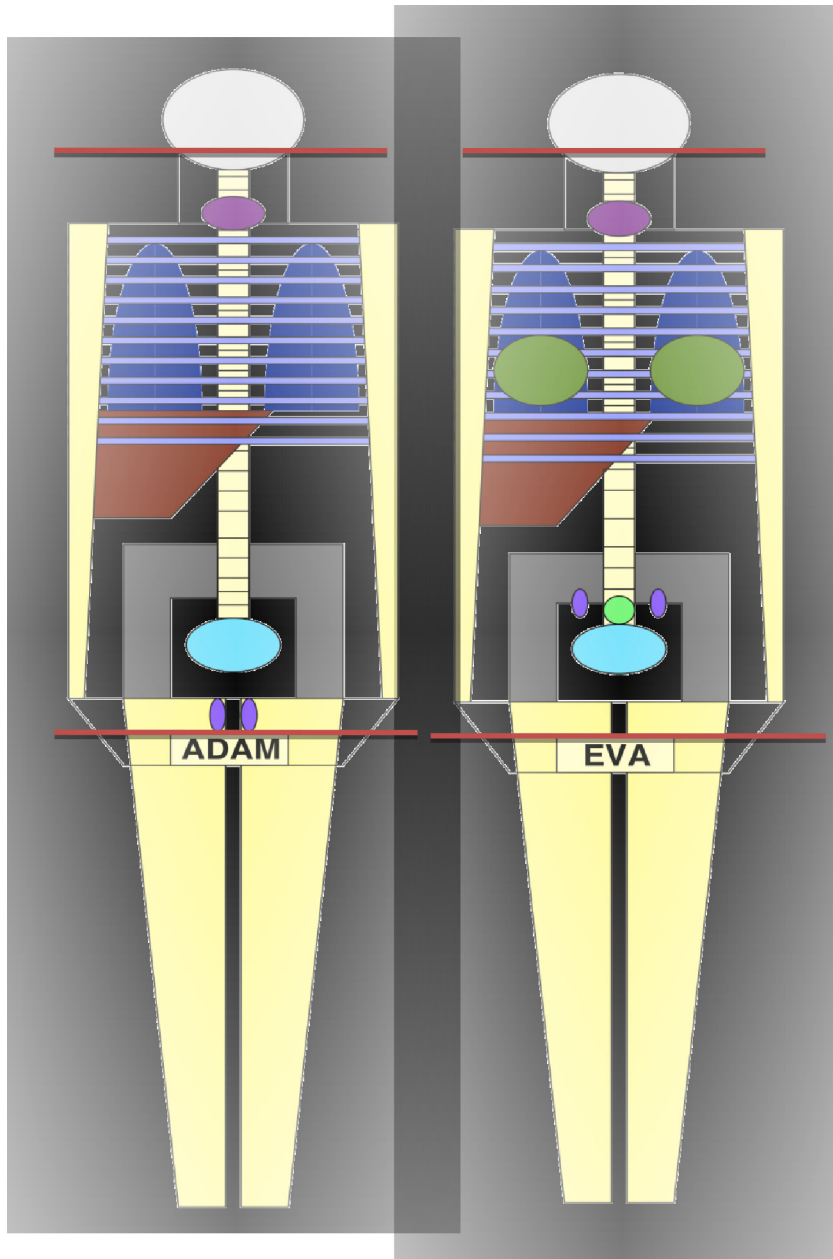


Figure 4.1: The ADAM and EVA phantoms of “CT-expo” used for CT dosimetry calculations: the division corresponds to the anatomical length of scan region

4.3.3 Internal dosimetry

The average activity (A) of ^{18}F -FDG administered for adults (male and female) was assumed to be 305 MBq (8.2mCi) [20]. This activity has an uptake time of 60min with intravenous contrast given. Equivalent dose, D_T to a tissue or organ T from the administered activity A of ^{18}F -FDG was computed by means of dose coefficients provided by the International Commission on Radiological Protection (ICRP) Publication 106 [21] for a variety of organs and tissues of the adult hermaphrodite MIRD (Medical Internal Radiation Dose) phantoms, using

$$D_T = A \cdot \Gamma_T^{FDG} \quad (4.1)$$

Whole body effective dose contribution from ^{18}F -FDG PET was then estimated as reported by Huang et al.[8] and Brix et al.[22] from organ and tissue equivalent doses D_T modified by tissue weighting factors in ICRP publication 103[20] as follows

$$E = \sum_T W_T \cdot D_T = A \cdot \sum_T W_T \cdot \Gamma_T^{FDG} \quad (4.2)$$

4.3.4 Data analysis

The total effective dose $ED_{PET/CT}$ values resulting from each systems and acquisition protocols were compared in terms of percentage differences calculated as describe by Eqn (4.3) below

$$\%DIFF(ED_{PET/CT}) = \left| \frac{ED_{syI} - ED_{syII}}{(ED_{syI} + ED_{syII})/2} \right| \times 100 \quad (4.3)$$

The difference in the CT component contribution to the total dose between the two systems for all protocols was assessed with an unpaired t-test. A p-value below 0.05 was considered statistically significant.

4.4 Results

Organs and Tissues equivalent dose D_T from administered ^{18}F -FDG activity and their contribution $W_T * D_T$ to the average PET scan effective dose 5.40mSv is reported in (Table 4.2). D_T ranged from 2.38 - 39.65mSv. Significant equivalent doses 20.44, 11.59, 6.41 and 6.10 mSv were to the heart, brain, liver, and lungs due to their relatively higher metabolic activity and hence rapid blood supply resulting in higher ^{18}F -FDG uptake [9]. The highest absorbed dose 39.65mSv to the bladder is attributed primarily to the final accumulation of the ^{18}F -FDG tracer in the urine in the urinary bladder, since the tracer is excreted by the kidney [23].

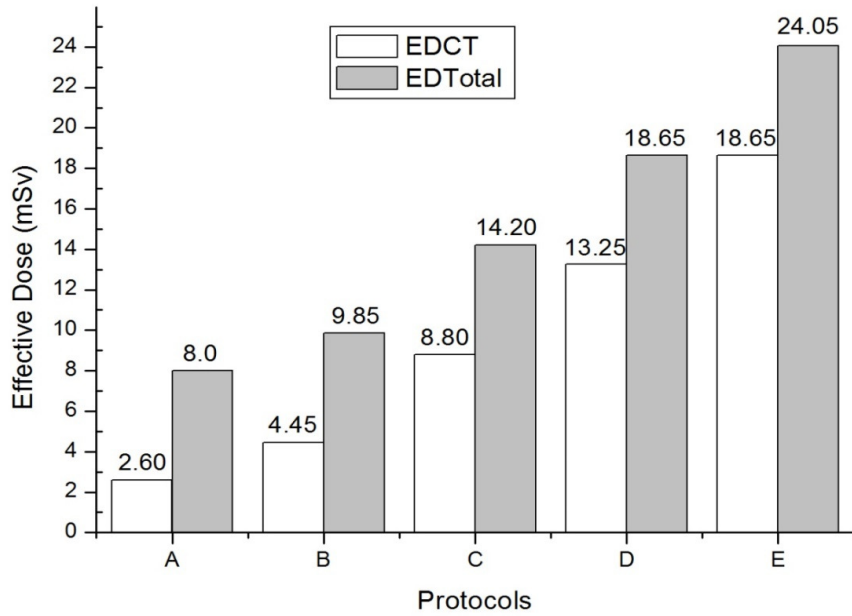
Figure (4.2) shows effective dose values from the five study protocols. The second column in each figure represents total effective dose ED from the PET-CT examination, considering CT contribution with ICRP 103 tissue weighting factors. The total ED of the combined PET-CT scan were 8.0, 9.85, 14.20, 18.65, 24.05 mSv for System I and 8.35, 11.45, 13.45, 17.90, 26.85 mSv, for System II for protocols A, B, C, D, and E respectively. The percentage differences in total ED values between the two Systems were 4.3%-15% for the Low-dose scan (A, B) and 4.1%-11% for standard dose scans (C-D). The CT effective doses contributions as seen in fig.4.2 were comparable for both systems, with two sample t-test results showing no significant differences ($p=0.885$; mean 9.55mSv for System I vs. 10.3mSv for system II). Statistical significance was defined as $p\text{-value} < 0.05$.

However, the slight differences observed in CT contribution resulted in higher total PET/CT dose for a specific system. For example, the ED from CT for low dose protocols A and B were 2.60 and 4.45mSv for system I, whereas the value was 2.95 and 6.05mSv for system II leading to variation of 12% and 30% between the two. Consecutively, the total PET/CT ED for System II was higher — 8.35 and 11.45mSv, in contrast to 8.0 and 9.85mSv for System I.

Table 4.2: Organs and Tissues equivalent dose D_T from administered ^{18}F -FDG activity and their contribution $W_T * D_T$ to the average PET effective dose

Organs	Dose Coefficient mSv/MBq	Organ Dose D_T mSv	$W_T * D_T$. mSv
Adrenals	0.012	3.66	0.031
Bladder	0.13	39.65	1.568
Bone surfaces	0.011	3.36	0.034
Brain	0.038	11.59	0.116
Breast	0.0088	2.68	0.322
Gallbladder	0.013	3.97	0.034
Stomach	0.011	3.36	0.403
Small intestine	0.012	3.66	0.031
Colon	0.013	3.97	0.476
Heart	0.067	20.44	0.175
Kidneys	0.017	5.19	0.044
Liver	0.021	6.41	0.256
Lungs	0.02	6.1	0.732
Muscles	0.01	3.05	0.026
Oesophagus	0.012	3.66	0.146
Ovaries	0.014	4.27	0.171
Pancreas	0.013	3.97	0.034
Red Marrow	0.011	3.36	0.403
Skin	0.0078	2.38	0.024
Spleen	0.011	3.36	0.029
Testes	0.011	3.36	0.134
Thymus	0.012	3.66	0.031
Thyroid	0.01	3.05	0.122
Uterus	0.018	5.49	0.047

(A)



(B)

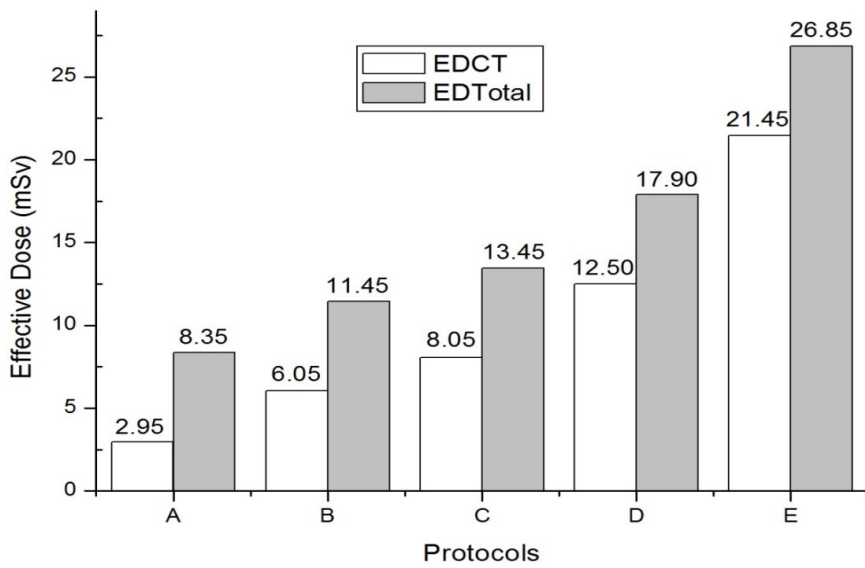


Figure 4.2: Mean Effective Dose values for Systems I (A) and II (B), calculated by applying the ICRP 103 tissue weighting factors.

4.5 Discussion

In this study, the effect of CT model and protocols on total dose from a PET-CT procedure was evaluated. Computed tomography (CT) acquisition in PET-CT imaging, is often performed for a variety of purposes, which includes diagnosis, anatomic localization and attenuation correction of the PET images [24]. However, there are possibilities of unnecessary exposure to high level of radiation dose, especially for CT imaging prescribed for diagnostic purposes.

The lower patient-specific effective dose 5.40mSv from the administered average FDG activity of 305 MBq (8.2mCi) in this study, compared to values of 6.25mSv and 6.28mSv reported by Dan Liu et al.[25] and Huang et al [8] respectively, is expected due to the greater FDG activities (328.77 and 370MBq) from these studies. Analysis of the effective dose ED derived from the CT component for systems and protocols considered in this study reveals that while the ED was within the 25.0mSv reported in the literature [8,22], ED values varied between 2.60-18.65mSv for the system I and 2.95-21.85mSv for system II with the ICRP 60 and 103 tissue-weighting factors.

As such, the CT component of the exam contributed between (32 -77%) for the system I and (35-79%) for system II of the whole radiation dose. These are somewhat comparable with the 17-76% range from a review of CT protocols and CT dose contribution in PET/CT [26] and with a study by Mahmud et al. [27], in which approximately 80.43% of the total PET/CT effective dose was attributable to the CT doses. It is worth pointing out that, for each system, the relatively low dose (typically less than 6% of the total dose [22]) from CT scout scan to select the scan region and establish bed positions for PET acquisition is not explicitly taken into account when considering the CT dose contribution. The observed differences between the two systems could be attributed to factors related to scanner geometry

and design (beam filtration, beam-shaping filter) and most importantly the user-adjustable factors (tube current and voltage, pitch factor, exposure time per rotation and slice collimation). A short-geometry scanner following the inverse square law radiation intensity varies inversely as the square of the distance between radiation source and patient, will produce more dose to the patient than a long geometry scanner [28]. The total beam filtration (inherent + added) of varying material and thickness absorbs via photoelectric interactions the output photons at a function of their energy [29-30]. These filters are noted for reducing radiation dose especially in the peripheral region of a field-of-view (FOV) [29, 32].

The most significant contributing factors to the disparities in estimated CT doses between the two systems from our study is perhaps the user-selectable parameters specifically the tube current-time product (mAs), pitch factor and collimation settings. Given the linear relationship between the tube current-time product (mAs) per rotation and the absorbed radiation dose [33], the choice of mAs has a major effect on the radiation dose from any CT examinations. The pitch (ratio of table feed per gantry rotation to the total collimated width of the X-ray beam) is inversely proportional to radiation dose if other scanning parameters are kept unchanged [28,32]. Therefore a higher pitch (Faster table speed for a given collimation) will decrease radiation dose because of a shorter exposure time. The system I had a higher pitch factor compared to system II, which might explain its lower effective dose. The lower dose from protocols (C and D) in system II than I, mean that the effect of an increase in dose with the use of lower pitch factor is slightly compensated by the use of the lower current-time product (mAs). Additionally, overranging (unnecessary radiation exposure outside the planned scan length), an effect directly proportional to the pitch, beam collimation and reconstructed slice thickness is also a possible contributor to the observed difference in CT dose, given the dissimilarities in these technical parameters Tables 4.1a and 4.1b for the two systems. The PET/CT effective doses from the two systems in this

study are similar to previous measures reported in the literature [8, 22, 33], with noticeable differences caused by the type of PET/CT scanner and protocol used in image acquisition. The radiation dose from a PET/CT scan depends on the PET/CT protocol, the patient's size and physiology, the amount of injected activity and the make and model of the PET/CT scanner. The PET effective dose is modest and depends on the activity of the injected FDG (^{18}F -Fluoro deoxy-glucose) which is the same whether a part of the body or the whole body is imaged. Major reductions in PET/CT dose is achieved from the CT component through the use of techniques such as automatic tube current modulation, iterative reconstruction, and adaptive filtering. Different vendors suggest different dose reduction methods; therefore every institution needs to develop scanner-specific protocols for implementing those methods. The estimated dose presented in this study comes with some limitations. First, Patient and organ dose calculations from CT with "CT-EXPO" v 2.4 are based on anthropomorphic mathematical models for a standard person that do not consider individual patients body sizes, organ positions and dimensions [34]. Different patient diameter, the divergent location of relevant organs may cause different radiation absorption and hence some discrepancies in reported estimates. However, they are a reasonably good indicator to checking the relative compliance with reference dose values and for scan protocols optimization [35]. Accordingly, the use is justified for the purpose of our study as we did not intend to estimate doses for individual patients, rather evaluate the overall radiation dose resulting from CT protocol and model change. Second, dose estimation was based on mean tube current values, because CT-Expo neglects the different approaches of automatic exposure control (AEC) methods operating with tube current modulation implemented on CT component. Use of AEC systems is likely to lower patient dose, but the magnitude of such dose savings has no substantial effect on the effective dose values [36]. Finally, the dose coefficients used for internal absorbed dose assessment were based on numerous assumptions [37] that may result

in variation from the “true” value.

4.6 Conclusions

The present study explored the effects of CT model and scan protocols on the overall dose from an ^{18}F -FDG PET/CT procedure based on CT exam-specific parameters with the CT-Expo dosimetry software. There is evidence of a slight variation in the effective dose contribution from the CT component for both PET/CT systems due to clinical technique differences and type of scanners. The presented dosimetric results also showed that radical changes to existing CT protocols are not necessary given that the total PET/CT dose from the two systems was typically within acceptable limits compared to current literature. Though the present work is just one step in the direction of a complete ED estimate that uses the exposure settings of all X-ray pulses, CT protocol optimization measures and patient weight specific ED contributions, the observed variations in CT dose is however of concern as the substantial radiation exposure of PET/CT imaging is from the CT examination. The absence of a diagnostic reference level (DRL) to promote optimization in PET/CT imaging, makes any decision regarding the need for optimization seems questionable. Further extended studies are needed to assess if a reduction in radiation exposure from the CT component, either by evaluating the current operator prescribed noise index level or by considering other diagnostic modalities such as limited CT scan length while keeping the diagnostic quality at a clinically acceptable level to reduce the probability of stochastic effects is possible.

ETHICAL APPROVAL

This article does not contain any studies with human participants performed by any of the authors.

Acknowledgments

This work was funded by the authors from research allowance given to academic staff of the University of KwaZulu-Natal.

Bibliography

- [1] Hahm CR, Park HY, Jeon K, Um SW, Suh GY, Chung MP, Kim H, Kwon OJ, W.J. Koh WJ (2010) Solitary Pulmonary Nodules Caused by Mycobacterium tuberculosis and Mycobacterium avium Complex. Lung.188: 25–31.
- [2] Skoura E, Zumla A, Bomanji J (2015) Imaging in tuberculosis. Int. J. Infect Dis. 32: 87–93
- [3] Kim IJ, Lee JS, Kim SJ, Kim YK, Jeong YJ, Jun S, Nam HY, Kim JS (2008) Double-phase ^{18}F -FDG PET–CT for determination of pulmonary tuberculoma activity. Eur. J. Nucl Med Mol. Imaging 35: 808-814.
- [4] Goo JM, Im JG, Do KH, Yeo JS, Seo JB, Kim HY, Chung JK (2000) pulmonary tuberculoma evaluated by means of FDG PET: findings in 10 cases. Radiology 216:117-121.
- [5] Karam M, Roberts-Klein S, Shet N, Chang J, Feustel P (2008) Bilateral hilar foci on ^{18}F -FDG PET scan in patients without lung cancer: variables associated with benign and malignant etiology. J Nucl. Med. 49:1429-1436.
- [6] Alessio AM, Kinahan PE, Cheng PM, Vesselle H, Karp JS (2004) PET/CT scanner instrumentation, challenges, and solutions. Radiol. Clin. North Am 42:1017-1032.

- [7] Soussan M, Brillet PY, Mekinian A, Khafagy A, Nicolas P, Vessieres A, Brauner M (2012) Patterns of pulmonary tuberculosis on FDG-PET/CT. *Eur. J. Radiol.*81: 2872-2876.
- [8] Huang B, Law MW, Khong PL (2009) Whole-Body PET/CT Scanning: Estimation of radiation dose and cancer risk. *Radiology* 251: 166-174.
- [9] Kaushik A, Jaimini A, Tripathi M, D'Souza M, Sharma R, Mishra AK, Mondal A, Dwarakanath BS (2013) Estimation of patient dose in ^{18}F -FDG and ^{18}F -FDOPA PET/CT examinations. *J. Cancer Res Ther.* 9: 477-483.
- [10] International Atomic Energy, Austria, (2013) Radiation protection of patients (RPOP). <https://rpop.iaea.org/RPOP/RPoP/Content/InformationFor/HealthProfessionals/index.htm>. Accessed 11 April 2017
- [11] Kumar S, Pandey AK, Sharma P, Malhotra A, Kumar R (2012) Optimization of the CT acquisition protocol to reduce patient dose without compromising the diagnostic quality for PET-CT: a phantom study. *Nucl Med Commun.* 33: 164-170.
- [12] Churchyard GJ, Mametja LD, Mvusi L, Ndjeka N, Hesseling AC, Reid A, Babatunde S, Pillay Y (2014) Tuberculosis control in South Africa: Successes, challenges, and recommendations. *South African Medical Journal*, 104: 244-248.
- [13] World Health Organization (2016) Global Tuberculosis Report. <http://www.who.int/iris/bitstream/10665/250441/1/9789241565394-eng.pdf>. Accessed 06 April 2017
- [14] Wall BF(1996) How to assess the dose to the patient in diagnostic radiology. National Radiation Protection Board NRPB, Chilton, Didcot, UK.

- [15] McCollough CH, Schueler BA(2000) Calculation of effective dose. *Med Phys.* 27:828-837.
- [16] Mettler FA, Huda W, Yoshizumi TT, Mahesh M (2008) Effective doses in radiology and diagnostic nuclear medicine: a catalog. *Radiology* 248: 254-263.
- [17] Inoue Y, Nagahara K, Tanaka Y, Miyatake H, Hata H, Hara T(2015) Methods of CT Dose Estimation in Whole-Body ^{18}F -FDG PET/CT. *J Nucl Med.* 56:695–700
- [18] Kramer R, Zankl M, Williams G, Drexler G(1982) The Calculation of Dose from external photon Exposures using reference human phantoms and Monte Carlo methods Part I. GSF-Report S-885.
- [19] ICRP (2007) The 2007 Recommendations of the International Commission on Radiological Protection. ICRP Publication 103 *Ann ICRP* 37: 2-4
- [20] Sathekge MM, Vorster M, Stoltz A, Jacobs AG (2014) Imaging of Pulmonary Tuberculosis with ^{18}F -Fluoro-Deoxy-Glucose and ^{18}F - Ethylcholine. *Open Nuclear Medicine Journal* 6:16-17.
- [21] ICRP (2008) Radiation dose to patients from radiopharmaceuticals Addendum 3 to ICRP Publication 53. ICRP Publication 106. *Annals ICRP* 38: 1-197.
- [22] Brix G, Lechel U, Glatting G, Ziegler SI, Munzing W, Muller SP, Beyer T(2005) Radiation Exposure of Patients Undergoing whole body Dual Modality Examinations. *J Nucl Med* 46:608-613.
- [23] Moran JK, Lee HB, Blafox MD (1999) Optimization of urinary FDG excretion during PET imaging. *J Nucl Med.* 40:1352–1357.
- [24] Alessio AM, Kinahan PE (2012) CT Protocol Selection in PET-CT Imaging-image wisely. *American College of Radiology.*

- [25] Liu D, Khong LP, Gao Y, Mahmood U, Quinn B, St.Germain J, Xu XG, Dauer LT (2016) Radiation Dosimetry of Whole-Body Dual-Tracer ^{18}F -FDG and ^{11}C -Acetate PET/CT for Hepatocellular Carcinoma. *J Nucl Med* 57:907–912
- [26] Vandevorode C(2011) CT Protocols and CT Dose Contribution in PET/CT. Department of Medical Physics and Radiation Protection, Ghent University.
- [27] Mahmud MH, Nordin AJ, Ahmad Saad FF, Fattah Azman AZ(2014) Estimation of patient radiation dose from whole body ^{18}F -FDG PET/CT examination in cancer imaging: a preliminary study. *J. Phys. Conf. Ser.* doi:10.1088/1742-6596/546/1/012008
- [28] Kalra MK, Maher MM, Toth TL, Hamberg LM, Blake MA, Shepard JA, Saini S. (2004) Strategies for CT radiation dose optimization. *Radiology.* 230:619-628
- [29] Euclid Seeram (2009) computed tomography physical principles, clinical applications, and quality control. 3rd edition. Saunders, USA.
- [30] Anders brahme (2014) Comprehensive Biomedical Physics, Volume 1. Elsevier B.V, USA, pp 28-29
- [31] Liu F, Wang G, Cong W, Hsieh SS, Pelc NJ (2013) Dynamic bowtie for fan-beam CT. *J Xray Sci Technol.* 21(4):579-590
- [32] Coursey CA, Frush DP (2008) CT and Radiation: What radiologists should know. *Appl Radiol.* 37(3):22-29
- [33] Khamwan K, Krisanachinda A, Pasawang P (2010) THE determination of patient dose from ^{18}F -FDG PET/CT examination. *Radiat Prot.Dosimetry.*141(1):50–55

- [34] Li X, Samei E, Segars WP, Sturgeon GM, Colsher JG, Toncheva G et al (2011) Patient-specific radiation dose and cancer risk estimation in CT: part II Application to patients. *Med Phys* 38:408–420
- [35] Reiser MF, Hricak H, Knauth M (2012) *Radiation dose from Multidetector CT*. 2nd edition. Springer-Verlag, Berlin, pp 565-566.
- [36] Lechel U, Becker G, Langenfeld-Jäger G, Brix G (2009) Dose reduction by automatic exposure control in multi-detector computed tomography: comparison between measurement and calculation. *Eur Radiol*.19:1027–1034
- [37] Hays MT, Watson EE, Thomas SR, Stabin M (2002) MIRD Dose Estimate Report No. 19: Radiation Absorbed Dose Estimates from ¹⁸F-FDG. *J Nucl Med* 43:210–214

Chapter 5

Conclusion and future work

5.1 Summary

This study was conducted to evaluate the radiation dose and the associated cancer risks from two imaging techniques (CT and PET-CT) predominantly employed in the diagnosis of Mycobacterium tuberculosis infections. The current rapid increase in usage, the relatively higher dose in comparisons to other imaging modalities and the varying degrees of difficulty in the appropriate selection of imaging protocol by radiologists due to variations in equipment design among manufacturers and models formed the basis for this study. The organ doses from CT scan were simulated using a dosimetry calculator taking into consideration adjustable scan parameters that are determinants of the amount of radiation a patient receives. Some of these factors include the tube current, the tube voltage measured in kilovolt peak, the pitch, display field of view etc., while doses from the PET scan were estimated applying the International Commission on Radiological Protection (ICRP) dose coefficients. Cancer risks, in the form of lifetime attributable risk (LAR) of cancer incidence, were estimated

by linear extrapolation using the organ radiation doses and the BEIR VII age-and-gender – dependent dose-risk model.

Our results on what potential harm, if any, does the use of generic protocols has on the absorbed radiation dose and long-term effects (cancer risks) for exposed patients showed percentage differences of 34% to 37% among the calculated effective dose (De) values for the scanners considered. The variability of associated lifetime cancer risks among the scanners was found to be slightly less than 1%. This related increase in cancer when applied to an increasingly large population with the proliferation of CT scanners in hospitals and institutions is a potential public health problem thus mandating careful patient selection and imaging protocol optimization by the radiologists to prevent unnecessary radiation.

The investigation of the influence of specific CT models and protocols on the overall PET/CT dose showed non-significant variations in PET/CT dose for the two systems examined. However, the influence of CT models and protocols were evident in the CT dose contributions as there were differences of up to 30% in the CT effective dose (De) values which in turn resulted in higher PET/CT dose for a particular system compared to the other.

This is primarily due to differences in technical parameters such as the tube potential, current-time product, scanning time, collimation etc. selected by the radiology personnel. Settings for CT should be selected to optimize pertinent diagnostic information that is the image quality must be balanced with radiation exposure taking economic and social issues into consideration. More importantly, the variations also demonstrate the importance of regular participation of radiographic staff in dose awareness training and dedicated teaching activities, with the purpose of improving clinical practices, enhancing quality of radiographs and minimising the amount of radiation exposure to patients.

5.2 Future work

As conversed in the study, our discussion related to radiation is an approximation of dose and is based on the CT acquisition parameters that directly affect the amount of radiation exposure a patient receives and over which the radiologist has direct control. Body size and patient-specific anatomy are overlooked with the use of physical phantoms and mathematical phantoms. Further research with more patient-specific methods to estimate organ and effective doses could lead to a more accurate reflection of the patient dose. However, any estimation of the effective dose that uses population-based ICRP weighting factors cannot be entirely patient-specific.

Moreover, the investigation on the influence of CT models and protocols on overall PET/CT dose was performed only for two PET/CT systems, which may not be applicable to regions that have different conditions regarding scanner equipment and cultural background of medical imaging. Given the limits of the sample size, machine parameters, these results should be interpreted within the context of this study. Future studies elsewhere will be of value to corroborate these findings.